J|A|C|S
ARTICLES
Published on Web 00/00/0000

A New Thermoelectric Material: $CsBi_4Te_6$

Duck-Young Chung,[†] Tim P. Hogan,[‡] Melissa Rocci-Lane,[§] Paul Brazis,[§] John R. Ireland,[§] Carl R. Kannewurf,[§] Marina Bastea,[||] Ctirad Uher,[||] and Mercouri G. Kanatzidis*[,†]

Contribution from the Department of Chemistry and Center for Fundamental Materials Research, and Department of Electrical & Computer Engineering and Materials Science and Mechanics, Michigan State University, East Lansing, Michigan 48824, Department of Electrical and Computer Engineering, Northwestern University, Evanston, Illinois 60208, and Department of Physics, University of Michigan, Ann Arbor, Michigan 48109

Received December 1, 2003; E-mail: kanatzidis@chemistry.msu.edu

Abstract: The highly anisotropic material $CsBi_4Te_6$ was prepared by the reaction of Cs/Bi_2Te_3 around 600 °C. The compound crystallizes in the monoclinic space group $C2/m$ with $a = 51.9205(8)$ Å, $b = 4.4025(1)$ Å, $c = 14.5118(3)$ Å, $\beta = 101.480(1)°$, $V = 3250.75(11)$ Å^3, and $Z = 8$. The final R values are $R_1 = 0.0585$ and $wR_2 = 0.1127$ for all data. The compound has a 2-D structure composed of NaCl-type $[Bi_4Te_6]$ anionic layers and Cs^+ ions residing between the layers. The $[Bi_4Te_6]$ layers are interconnected by Bi−Bi bonds at a distance of 3.2383(10) Å. This material is a narrow gap semiconductor. Optimization studies on the thermoelectric properties with a variety of doping agents show that the electrical properties of $CsBi_4Te_6$ can be tuned to yield an optimized thermoelectric material which is promising for low-temperature applications. SbI_3 doping resulted in p-type behavior and a maximum power factor of 51.5 $\mu W/cm\cdot K^2$ at 184 K and the corresponding ZT of 0.82 at 225 K. The highest power factor of 59.8 $\mu W/cm\cdot K^2$ at 151 K was obtained from 0.06% Sb-doped material. We report here the synthesis, physicochemical properties, doping characteristics, charge-transport properties, and thermal conductivity. Also presented are studies on n-type $CsBi_4Te_6$ and comparisons to those of p-type.

Introduction

$Bi_{2-x}Sb_xTe_{3-y}Se_y$ alloys,[1] the currently leading thermoelectric materials for room-temperature cooling applications, have been used for decades as their thermoelectric performance has reached optimal values through optimization of composition,[2] doping,[3] and device design. There are now considerable demands in identifying new materials with more enhanced thermoelectric properties than those exhibited by currently employed materials.[4,5] Particularly, interesting are candidate materials that could exceed the performance characteristics of $Bi_{2-x}Sb_xTe_{3-y}Se_y$ alloys at or below room temperature. To date, exploration for new materials has focused on several chemical systems such as ternary chalcogenides,[6,7] skutterudites,[8] half-heusler alloys,[9] clathrates,[10] and pentatellurides.[11]

The challenge for superior thermoelectric materials lies in achieving simultaneously high electrical conductivity, high thermoelectric power, and low thermal conductivity. These

[†] Department of Chemistry and Center for Fundamental Materials Research, Michigan State University.
[‡] Department of Electrical & Computer Engineering and Materials Science and Mechanics, Michigan State University.
[§] Northwestern University.
[||] University of Michigan.

(1) (a) Testardi, L. R.; Bierly, J. N., Jr.; Donahoe, F. J. *J. Phys. Chem. Solids* **1962**, *23*, 1209. (b) Champness, C. H.; Chiang, P. T.; Parekh, P. *Can. J. Phys.* **1965**, *43*, 653−659; (c) **1967**, *45*, 3611−3626. (d) Jeon, H.-H.; Ha, H.-P.; Hyun, D.-B.; Shim, J.-D. *J. Phys. Chem. Solids* **1991**, *4*, 579−585.
(2) (a) Yim, W. M.; Fitzke, E. V. *J. Electrochem. Soc.* **1968**, *115*, 556−560. (b) Yim, W. M.; Fitzke, E. V.; Rosi, F. D. *J. Mater. Sci.* **1966**, *1*, 52−65. (c) Borkowski, K.; Przyluski, J. *Mater. Res. Bull.* **1987**, *22*, 381−387.
(3) (a) Chizhevskaya, S. N.; Shelimova, L. E. *Inorg. Mater.* **1995**, *31*, 1083−1095. (b) Horák, J.; Cermák, K.; Koudelka, L. *J. Phys. Chem. Solids* **1986**, *47*, 805−809. (c) Lostak, P.; Horák, J.; Koudelka, L. *Phys. Status Solidi* **1983**, *76*, k71−k75. (d) Zalar, S. M. *Adv. Energy Convers.* **1962**, *2*, 105−112.
(4) (a) *Chemistry, Physics, and Materials Science of Thermoelectric Materials − Beyond Bismuth Telluride*; Kanatzidis, M. G., Mahanti, S. D., Hogan, T. P., Eds. (New Thermoelectric Materials Workshop Proceedings, Traverse City, MI, 2002); In *Fundamental Materials Research Series*; Thorpe, M. F., Ed.; Kluwer Academic/Plenum Publishers: New York, 2003. (b) Mrotzek, A.; Kanatzidis, M. G. *Acc. Chem. Res.* **2003**, *36*, 111−119. (c) Thermoelectric Materials − New Directions and Approaches. *Materials Research Society Symposium Proceedings*; Tritt, T. M., Kanatzidis, M. G., Lyon, H. B., Mahan, G. D., Eds.; Materials Research Society: PA, 1997; Vol. 478.
(5) Chung, D.-Y.; Hogan, T.; Schindler, J.; Iordanidis, L.; Brazis, P.; Kannewurf, C. R.; Chen, B.; Uher, C.; Kanatzidis, M. G. In *Materials Research Society Symposium Proceedings*; Tritt, T. M., Kanatzidis, M. G., Lyon, H. B., Mahan, G. D., Eds.; Materials Research Society: PA, 1997; Vol. 478, pp 333−344.
(6) Chung, D.-Y.; Choi, K.-S.; Iordanidis, L.; Schindler, J. L.; Brazis, P. W.; Kannewurf, C. R.; Chen, B.; Hu, S.; Uher, C.; Kanatzidis, M. G. *Chem. Mater.* **1997**, *9*, 3060−3071.
(7) (a) Wood, C. *Rep. Prog. Phys.* **1988**, *51*, 459−539. (b) Christakudis, G. Ch.; Plachkova, S. K.; Shelimova, L. E.; Avilov, E. S. *Phys. Status Solidi A* **1991**, *128*, 465−471. (c) Shelimova, L. E.; Avilov, E. S.; Kretova, M. A. *Inorg. Mater.* **1994**, *30*, 1165−1172; **1993**, *29*, 961−964.
(8) (a) Sales, B. C.; Mandrus, D.; Williams, R. K. *Science* **1996**, *272*, 1325−1328. (b) Chen, B. X.; Xu, J. H.; Uher, C.; Morelli, D. T.; Meisner, G. P.; Fleurial, J.-P.; Caillat, T.; Borshchevsky, A. *Phys. Rev. B* **1997**, *55*, 1476−1480.
(9) (a) Uher C.; Yang, J.; Hu, S.; Morelli, D. T.; Meisner, G. P. *Phys. Rev. B* **1999**, *59*, 8615. (b) Hohl, H.; Ramirez, A. P.; Goldmann, C.; Ernst, G.; Wölfing, B.; Bucher, E. *J. Phys.: Condens. Matter* **1999**, *11*, 1697. (c) Kafer, W.; Fess, K.; Kloc, C.; Friemelt, K.; Bucher, E. *Inst. Phys. Conf. Ser.* **1998**, *152*, 185−188.

properties define the thermoelectric figure of merit $ZT = (S^2\sigma/\kappa)T$, where S is the thermopower, σ is the electrical conductivity, κ is the thermal conductivity, and T is the temperature. All three of these parameters are not independently controllable because they are determined by the details of the electronic structure and the charge carrier-related properties such as mobility, carrier concentration, effective mass, and scattering time. The thermal conductivity (κ) also has two contributions, one from carriers (κ_e) and one from lattice vibrations (κ_l). The latter is in principle independently controllable through chemical manipulation.

Materials with more complex composition and structure may have complex electronic structures, which may give rise to high thermoelectric power and at the same time low thermal conductivity. The Boltzmann transport theory provides a general understanding of thermopower using the Mott formula:

$$S = \frac{\pi^2}{3} \cdot \frac{k^2 T}{e} \cdot \frac{\mathrm{d} \ln \sigma(E)}{\mathrm{d}E}\Big|_{E=E_f}$$

The conductivity, $\sigma(E)$, is determined as a function of band filling or Fermi energy, and the thermopower, S, is just proportional to the logarithmic derivative of $\sigma(E)$ with respect to E near the Fermi surface. This implies that the thermopower of a material is a measure of the asymmetry in electronic structure and scattering rates near the Fermi energy, suggesting one can control simultaneously σ and S by manipulating the energy dependence of $\sigma(E)$. Another desirable way to increase ZT is to minimize κ_l while retaining good electrical and thermopower properties.

Our approach to searching for new thermoelectrics has been to build new structures from alkali metals, bismuth and chalcogen atoms. We have reported on $BaBiTe_3$,[12] $KBi_{6.33}S_{10}$,[13] α-, β-, γ-$K_2Bi_8Q_{13}$ (Q = Se,[6,14,15] S[13]), $K_{2.5}Bi_{8.5}Se_{14}$,[6] and $KM_4Bi_7Se_{15}$ (M = Sn, Pb)[16] that show promising thermoelectric properties. Particularly, the compounds $K_2Bi_8Q_{13}$ (Q = Se, S) possess low symmetry and a large unit cell, with "loosely" bound K^+ ions in channels composed of covalently bonded Bi/Q blocks. The measured properties for these compounds suggest that low thermal conductivity and promising thermoelectric properties could be achieved by introducing alkali metals in the Bi/Q (Q = Te, Se, S) binary system. To investigate isostructural tellurium compounds, we focused on the Cs/Bi/Te system, which, however, gave an unexpected result where, instead of the $Cs_2Bi_8Te_{13}$ being observed, a reduced compound was isolated, $CsBi_4Te_6$, which can be viewed as containing Bi^{2+} ions that form novel Bi−Bi bonds.

In a preliminary communication,[17] we reported that appropriate p-type doping of $CsBi_4Te_6$ gives rise to a high ZT_{max} of 0.8 at 225 K. At this temperature, $CsBi_4Te_6$ is the best performing thermoelectric material and raises new hope for extending the use of thermoelectric materials to temperatures lower than ever before. Since then, we have identified a new dopant which allows the high ZT_{max} to be shifted to even lower temperatures in the neighborhood of 180 K. With the aid of electronic band structure calculations reported earlier,[18] we present a broad and in-depth discussion of the structure property relationships in this material. We present in detail here the synthesis, physicochemical, spectroscopic, and structural characterization of $CsBi_4Te_6$. We also report extensive doping studies including a complete set of thermoelectric properties, electrical conductivity, Seebeck coefficient, and thermal conductivity, for both p- and n-type $CsBi_4Te_6$ over a wide range of temperatures.

Experimental Section

Reagents. Chemicals in this work were used as obtained: (i) bismuth, 99.999% purity, Cerac, Milwaukee, WI; (ii) tellurium powder, 99.999% purity, Cerac, Milwaukee, WI; (iii) cesium metal, 99.98% purity, Johnson and Matthey Co., Ward Hill, MA; (iv) selenium, 99.999% purity, Cerac, Milwaukee, WI; (v) antimony, 99.999% purity, Cerac, Milwaukee, WI; (vi) Bi_2Te_3 was prepared by melting the stoichiometric mixture of Bi and Te at 800 °C; (vii) high purity commercial reagents were used for elemental dopants (Sn, Zn, Mg, Te); (viii) the dopant compounds were prepared as described in the literature[19] for SbI_3 and BiI_3, or by stoichiometric reactions of the elements at 750 °C for SnTe and In_2Te_3. These dopants were purified by sublimation before use.

Synthesis of $CsBi_4Te_6$. All premanipulations were carried out under a dry nitrogen atmosphere in a Vacuum Atmospheres Dri-Lab glovebox and in a Schlenk line. Cs_2Te was obtained by stoichiometric reactions of elemental cesium and tellurium in liquid NH_3.[20] It was dried and ground to give a fine homogeneous powder prior to use. $CsBi_4Te_6$ could be obtained in various ways as follows:

Method A. Cs_2Te (0.192 g, 0.488 mmol) and Bi_2Te_3 (0.6 g, 0.749 mmol) were thoroughly mixed and loaded into an alumina thimble (10 mm o.d. × 7 mm i.d. × 75 mm), which was plugged with a graphite lid and subsequently sealed inside a silica tube (13 mm o.d. × 11 mm i.d.) at a residual pressure of $<10^{-4}$ Torr. The mixture was heated to 300 °C over 24 h followed by heating to 700 °C at a rate of ∼3 °C/h. It was isothermed there for 2.5 days and then slowly cooled to 300 °C at a rate of −4 °C/h followed by cooling to 50 °C in 12 h. The product was isolated by dissolving away the residual Cs_2Te with several portions of degassed dimethylformamide under a nitrogen atmosphere until the solvent remained clear. After being washed with ether and dried, shiny long silvery needles of $CsBi_4Te_6$ were obtained in quantitative yield.

Method B. A mixture of Cs metal (0.033 g, 0.248 mmol) and Bi_2Te_3 (0.3 g, 0.375 mmol) was loaded in an alumina thimble. An exothermic reaction took place during mixing. The mixture was sealed by the same procedure as above and heated to 600 °C at a rate of 5 °C/h. The mixture was isothermed there for 1 day followed by slow cooling at a rate of −4 °C/h to 150 °C. The alumina thimble containing the product was immersed overnight in dried and degassed methanol under a nitrogen atmosphere. The relatively large crystals (>5 mm long) of $CsBi_4Te_6$ were taken out of the thimble by carefully scratching with a spatula and were washed with methanol.

(10) (a) Nolas, G.; Cohn, J. L.; Slack, G.; Schujman, S. B. *Appl. Phys. Lett.* **1998**, *73*, 178. (b) Nolas, G.; Slack, G.; Morelli, D. T.; Tritt, T. M.; Ehrlich, A. C. *J. Appl. Phys.* **1996**, *79*, 4002−4008.

(11) (a) Littleton, R. T., IV; Tritt, T. M.; Feger, C. R.; Kolis, J.; Wilson, M. L.; Marone, M.; Payne, J.; Verebeli, D.; Levy, F. *Appl. Phys. Lett.* **1998**, *72*, 2056. (b) Sharp, J. W.; Sales, C. B.; Mandrus, D. G.; Chakoumakos, B. C. *Appl. Phys. Lett.* **1999**, *74*, 3794.

(12) Chung, D.-Y.; Jobic, S.; Hogan, T.; Kannewurf, C. R.; Brec, R.; Rouxel, J.; Kanatzidis, M. G. *J. Am. Chem. Soc.* **1997**, *119*, 2505.

(13) Kanatzidis, M. G.; McCarthy, T. J.; Tanzer, T. A.; Chen, L.-H.; Iordanidis, L.; Hogan, T.; Kannewurf, C. R.; Uher, C.; Chen, B. *Chem. Mater.* **1996**, *8*, 1465−1474.

(14) McCarthy, T. J.; Ngeyi, S.-P.; Liao, J.-H.; DeGroot, D. C.; Hogan, T.; Kannewurf, C. R.; Kanatzidis, M. G. *Chem. Mater.* **1993**, *5*, 331−340.

(15) γ-$K_2Bi_8Se_{13}$: Chung, D.-Y.; Kyratsi, T.; Kanatzidis, M. G., unpublished results.

(16) Choi, K.-S.; Chung, D.-Y.; Mrotzek, A.; Brazis, P.; Kannewurf, C. R.; Uher, C.; Chen, W.; Hogan, T.; Kanatzidis, M. G. *Chem. Mater.* **2001**, *13*, 756−764.

(17) Chung, D.-Y.; Hogan, T.; Brazis, P.; Rocci-Lane, M.; Kannewurf, C. R.; Bastea, M.; Uher, C.; Kanatzidis, M. G. *Science* **2000**, *287*, 1024−1027.

(18) Larson, P.; Mahanti, S. D.; Chung, D.-Y.; Kanatzidis, M. G. *Phys. Rev. B* **2002**, *65*, 45205.

(19) (a) Bailar, J. C., Jr.; Cundy, P. F. In *Inorganic Syntheses*; Bailar, J. C., Jr., Ed.; McGraw-Hill Book Co. Inc.: New York, 1939; Vol. 1, p 104. (b) Watt, G. W.; Hakki, W. W.; Choppin, G. R. In *Inorganic Syntheses*; Booth, H. S., Ed.; McGraw-Hill Book Co. Inc.: New York, 1953; Vol. 4, p 114.

(20) (a) Klemm, W.; Sodomann, H.; Langmesser, P. *Z. Anorg. Allg. Chem.* **1939**, *241*, 281−304. (b) Feher, F. In *Handbuch der Praparativen Anorganischen Chemie*; Brauer, G., Ed.; Ferdinand Enke: Stuttgart, Germany, 1954; pp 280−281. (c) Sheldrick, W. S.; Braunbeck, H.-G. *Z. Naturforsch* **1990**, *45B*, 1643−1646.

Method C. A mixture of Cs metal (0.432 g, 3.250 mmol) and Bi_2Te_3 (5.0 g, 6.244 mmol) was loaded and sealed as above. The mixture was heated at 250 °C for 24 h to complete the reaction of Cs metal. The resulting black material mixed with unreacted Bi_2Te_3 was slowly melted in a flame torch for a minute and then quenched in air. This method also gives a quantitative yield and is suitable for a large-scale synthesis.

Method D. Cs metal (0.1 g, 0.752 mmol) and Bi_2Te_3 (1.0 g, 1.249 mmol) were loaded separately in the two ends of a H-shaped silica tube (13 mm o.d. × 11 mm i.d.). The other two ends were sealed under vacuum ($<10^{-4}$ Torr) while keeping the Cs-containing end in liquid N_2 temperature to avoid evaporation of the metal. The tube was heated to 250 °C over 24 h and isothermed there for 1 day followed by heating to 580 °C over 24 h. After 2 days at 580 °C, it was cooled to 50 °C in 12 h. The product obtained at 100% yield was washed with several portions of degassed methanol under nitrogen atmosphere.

The purity and homogeneity of the product obtained from each method were confirmed by comparison of the X-ray powder diffraction (XRD) pattern to that calculated from the single-crystal X-ray analysis. A quantitative analysis by energy dispersive spectroscopy (EDS) using a scanning electron microscope (SEM) was also performed on a large number of the $CsBi_4Te_6$ crystals and showed an average ratio of "$Cs_{0.96}$-$Bi_4Te_{6.6}$".

Doping $CsBi_4Te_6$. All doped materials were synthesized using doped Bi_2Te_3 as a starting material. To obtain doped Bi_2Te_3, each dopant was mixed with it and melted at 800 °C in a rocking furnace and quenched in air. In the cases of Bi and Sb doping, stoichiometrically doped $Bi_{2+x}Te_{3-x}$ and $Bi_2Sb_xTe_{3-x}$ ($x < 0.2$) were used as starting materials. The reaction of doped Bi_2Te_3 with Cs was performed by method D. After synthesis of the doped $CsBi_4Te_6$, crystal growth was carried out by a Bridgman technique to obtain well-oriented ingots. The ingots were then annealed at 250 °C for 2 days before measurements of charge-transport properties. A doping level in units of mol % was applied in this doping study.

Physical Measurements

Electron Microscopy. Quantitative microprobe analyses of the compound were performed with a JEOL JSM-35C scanning electron microscope (SEM) equipped with a Tracor Northern energy dispersive spectroscopy (EDS) detector. Data were acquired using an accelerating voltage of 20 kV and a 1-min accumulation time.

Differential Thermal Analysis. Differential thermal analysis (DTA) was performed with a computer-controlled Shimadzu DTA-50 thermal analyzer. The ground single crystals (~20 mg total mass) were sealed in a carbon-coated silica ampule under vacuum. A silica ampule containing alumina of equal mass was sealed and placed on the reference side of the detector. The samples were heated to 800 °C at 10 °C/min, then isothermed for 2 min followed by cooling at 10 °C/min to 100 °C and finally by rapid cooling to room temperature. The reported DTA temperature is the peak temperature. The DTA sample was examined by powder X-ray diffraction after the experiment.

Raman Spectroscopy. Raman spectra were recorded on a Holoprobe Raman spectrograph. The experimental details were reported elsewhere.[21]

Infrared Spectroscopy. Optical diffuse reflectance measurements were made on the finely ground sample at room temperature. The spectrum was recorded in the infrared region (6000−400 cm^{-1}) with the use of a Nicolet MAGNA-IR 750 spectrometer equipped with a collector diffuse reflectance of Spectra-Tech, Inc. Absorption (α/S) data were calculated from the reflectance data using the Kubelka−Munk function:[22] $\alpha/S = (1 - R)^2/2R$, where R is the reflectance at a given wavenumber, α is the absorption coefficient, and S is the scattering coefficient.

Charge-Transport Property Measurements. The crystals of $CsBi_4Te_6$ suitable for electrical conductivity and thermopower measurements typically exhibited lengths in the order of 1−10 mm along the needle axis that provided an excellent geometry for the measurements. DC conductivity measurements were performed in the usual four-probe geometry with 60- and 25-μm gold wires used for the current and voltage electrodes, respectively. Conductivity data were obtained with the computer-automated system described elsewhere.[23a] Thermoelectric power measurements were made by using a slow ac technique[23b] with 60-μm gold wires serving to support and conduct heat to the sample, as well as to measure the voltage across the sample resulting from the applied temperature gradient. In both measurements, the gold electrodes were held in place on the sample with a conductive gold paste.

Conductivity specimens were mounted on interchangeable sample holders, and thermopower specimens were mounted on a fixed sample holder/differential heater. Mounted samples were placed under vacuum (10^{-3} Torr) and heated to room temperature for 24 h to cure the gold contacts. For a variable-temperature run, data (conductivity or thermopower) were acquired during the warming cycle. The temperature drift rate during an experiment was kept below 1 K/min. For some samples, three to four separate variable-temperature runs were carried out to ensure reproducibility. At a given temperature, reproducibility was within ±5%.

Hall Effect Measurements. Mobility and carrier concentration data were obtained using dc Hall effect measurements from 4.2 to 340 K using a computer-controlled five-probe technique.[23] The voltage sensing electrodes were 25 μm diameter gold wire; the current electrodes were 60 μm diameter gold wire and were mounted across the ends of the samples. The electrode wires were attached to the sample with gold paste. For the $CsBi_4Te_6$ samples, contacts made with gold paste were found to be superior in most cases to those made with silver paste. Hall measurements were performed with a 7.4 kG magnetic flux density and typically with a 1 mA applied current. All voltages were measured using a Keithley 2182 nanovoltmeter. Some Hall measurements were carried out in a reduced pressure (~10 mTorr) atmosphere of dry helium gas to improve thermal equilibrium. The relationship $|R_H| = 1/ne$ was used for determining carrier concentrations, where R_H is the Hall coefficient, n is the carrier concentration, and e is the electronic charge.

Thermal Conductivity Measurements. (1) Thermal conductivity was determined using a longitudinal steady-state method over the temperature range 4−300 K. Samples were attached (using either a low melting point solder or a silver-loaded epoxy) to the cold tip of the cryostat, while the other end of the sample was provided with a small strain gauge

(21) Aitken, J. A.; Evain, M.; Iordanidis, L.; Kanatzidis, M. G. *Inorg. Chem.* **2002**, *41*, 180−191.

(22) (a) Wendlandt, W. W.; Hecht, H. G. *Reflectance Spectroscopy*; Interscience Publishers: New York, 1966. (b) Kotüm, G. *Reflectance Spectroscopy*; Springer-Verlag: New York, 1969. (c) Tandon, S. P.; Gupta, J. P. *Phys. Status Solidi* **1970**, *38*, 363−367.

(23) (a) Lyding, J. W.; Marcy, H. O.; Marks, T. J.; Kannewurf, C. R. *IEEE Trans. Instrum. Meas.* **1988**, *37*, 76−80. (b) Chaikin, P. I.; Kawk, J. F. *Rev. Sci. Instrum.* **1975**, *46*, 218−220.

resistor, which serves as a heater. The temperature difference across the samples was measured using a differential chromel−constantan thermocouple. (2) Thermal conductivity measurements were also obtained using a pulse technique developed by Maldonado.[24] The method was modified for a computer-controlled procedure by Hogan.[25] The technique allows both thermal conductivity and thermopower data to be recorded during the data collection cycle. For comparison, thermoelectric power measurements were also taken in the measurement system employing the slow-ac technique described above and showed good agreement with results from the pulse technique.

Crystallography. A single crystal of $CsBi_4Te_6$ with dimensions 0.028 mm × 0.051 mm × 0.307 mm was mounted on the tip of a glass fiber. Intensity data were collected at 293 K on a Siemens SMART Platform CCD diffractometer using graphite monochromatized Mo Kα radiation over a full sphere of reciprocal space, up to 56.3° in 2θ. The individual frames were measured with an ω rotation of 0.3° and an acquisition time of 45 s. The SMART[26] software was used for the data acquisition, and SAINT[27] was used for data extraction and reduction. The absorption correction was done using SADABS.

Structure solution and refinement for the compound were done with the SHELXTL[28] package of crystallographic programs. Systematic absence conditions of the collected data suggested either the *C*2/*m*, *C*2, or *Cm* space group. Direct methods succeeded with the lower symmetry space group *Cm* (No. 8) and gave a reasonable structural model. This model possessed a center of inversion, and it was confirmed with the MISSYM algorithm[29] as implemented in the PLATON program,[30] suggesting the correct space group *C*2/*m*. Structure refinement in *C*2/*m* gave 4.34/10.17% of the final R_1/wR_2.

The complete data collection parameters and details of the structure solution and refinement for $CsBi_4Te_6$ are given in Table 1. The fractional coordinates and temperature factors (U_{eq}) of all atoms with estimated standard deviations are given in Table 2.

Results and Discussion

Synthesis and Physicochemical Properties. The challenge in exploring new alkali metal bismuth telluride compounds is the exceptional thermodynamic stability of Bi_2Te_3. Our investigation over a wide range of reaction conditions of the Cs/Bi/Te suggests that $CsBi_4Te_6$ is the only ternary compound in this system. Although a compound with a composition of $CsBiTe_2$ has been proposed,[31] it was not found at all in our investigations of the Cs/Bi/Te system. $CsBi_4Te_6$ could be prepared in a reaction of Cs_2Te and Bi_2Te_3 with a ratio of 0.65/1 at 650 °C for 1 day. Under such a condition, the highly reactive Cs_2Te breaks down Bi_2Te_3. This reaction is remarkable because the formation of $CsBi_4Te_6$ requires the formal reduction of Bi^{3+} to Bi^{2+} and concomitant oxidation of Te^{2-}. This is a rare and difficult redox reaction and unprecedented in A_2Q/Bi_2Q_3 (A = alkali metal; Q = chalcogen) reaction systems.[6,12−16] It is the first example in which Bi^{3+} is reduced in a bismuth chalcogenide compound forming a Bi−Bi bond (see below). That it happens at all attests to the high thermodynamic stability of $CsBi_4Te_6$. Interestingly, $CsBi_4Te_6$ is also unique in that it has neither alkali analogues (e.g., K, Rb) nor Sb or Se analogues. A small amount of Sb and Se can be added in the structure to form $CsBi_{4-x}Sb_xTe_6$ ($0 < x < 0.8$) and $CsBi_4Te_{6-y}Se_y$ ($0 < y < 1.2$), but complete substitution was found to be impossible.

Given that $CsBi_4Te_6$ is a reduced form of Bi_2Te_3, we also devised rational synthetic routes involving the direct combina-

Table 1. Summary of Crystallographic Data and Structural Analysis for $CsBi_4Te_6$

formula	$CsBi_4Te_6$
formula weight	1734.43
crystal habit	silvery white needle
crystal size, mm^3	0.028 × 0.051 × 0.307
space group	*C*2/*m* (No. 12)
a, Å	51.9205(8)
b, Å	4.40250(10)
c, Å	14.5118(3)
β, deg	101.4800(10)
Z; *V*, Å^3	8; 3250.75(11)
D_{calc}, gcm^{-3}	7.088
temp, K	293(2)
λ(Mo Kα), Å	0.71069
absorption coeff, mm^{-1}	55.899
F(000)	5592
$\theta_{min}-\theta_{max}$, deg	1.43−28.17
index ranges	$-68 \le h \le 68$, $-5 \le k \le 5$, $-19 \le l \le 18$
total reflns collected	18 450
independent reflns	4373 [*R*(int) = 0.0767]
refinement method	full-matrix least-squares on F^2
data/restraints/params	4373/0/134
final *R* indices [$I > 2\sigma(I)$][a,b]	$R_1 = 0.0434$, wR2 = 0.1017
R indices (all data)[a,b]	$R_1 = 0.0585$, wR2 = 0.1127
extinction coeff	0.000076(6)
largest diff. peak and hole, e·A^{-3}	4.344 and −2.490
GOF on F^2	1.050

[a] $R_1 = \sum||F_o| - |F_c||/\sum|F_o||$. [b] $wR_2 = \{\sum[w(F_o^2 - F_c^2)^2]/\sum[w(F_o^2)^2]\}^{1/2}$.

Table 2. Fractional Atomic Coordinates (×10^4) and Equivalent Atomic Displacement Parameter (A^2 × 10^3) for $CsBi_4Te_6$ with Estimated Standard Deviations in Parentheses

	x	*y*	*z*	*U*(eq)[a]
Bi(1)	1362(1)	0	7502(1)	17(1)
Bi(2)	2124(1)	5000	−888(1)	18(1)
Bi(3)	1628(1)	0	921(1)	18(1)
Bi(4)	886(1)	5000	−627(1)	18(1
Bi(5)	2353(1)	5000	−7410(1)	17(1
Bi(6)	1146(1)	5000	2782(1)	17(1)
Bi(7)	150(1)	0	7878(1)	18(1)
Bi(8)	396(1)	0	1365(1)	18(1)
Cs(1)	543(1)	0	5090(1)	26(1)
Cs(2)	3130(1)	0	−5163(1)	28(1)
Te(1)	1533(1)	5000	−722(1)	14(1)
Te(2)	800(1)	0	7845(1)	16(1)
Te(3)	1226(1)	5000	6089(1)	18(1)
Te(4)	2020(1)	0	7561(1)	16(1)
Te(5)	2250(1)	0	766(1)	14(1)
Te(6)	1043(1)	0	1003(1)	15(1)
Te(7)	1757(1)	5000	−7570(1)	16(1)
Te(8)	1236(1)	0	4213(1)	18(1)
Te(9)	2396(1)	0	−5982(1)	18(1)
Te(10)	575(1)	5000	2811(1)	18(1)
Te(11)	−76(1)	5000	3592(1)	19(1)
Te(12)	322(1)	5000	−383(1)	17(1)

[a] *U*(eq) is defined as one-third of the trace of the orthogonalized U_{ij} tensor.

(24) Maldonado, O. *Cryogenics* **1992**, *32*, 908−912.
(25) Hogan, T. P. Ph.D. Dissertation, Northwestern University, 1996.
(26) SMART: Siemens Analytical X-ray Systems, Inc.: Madison, WI, 1994.
(27) SAINT: Version 4, Siemens Analytical X-ray Systems, Inc.: Madison, WI, 1994−1996.
(28) Sheldrick, G. M. SHELXTL: Version 5; Siemens Analytical X-ray Systems, Inc.: Madison, WI, 1994.
(29) Le Page, Y. *J. Appl. Crystallogr.* **1987**, *20*, 264−269.
(30) Spek, A. L. *Acta Crystallogr., Sect. A* **1990**, *46*, C34.
(31) (a) Trippel, A. F.; Lazarev, V. B.; Berul, S. I. *Russ. J. Inorg. Chem.* **1978**, *23*, 390−392. (b) Even with a stoichiometric mixture targeting $CsBiTe_2$, the reactions led to $CsBi_4Te_6$ and Cs/Te impurity.

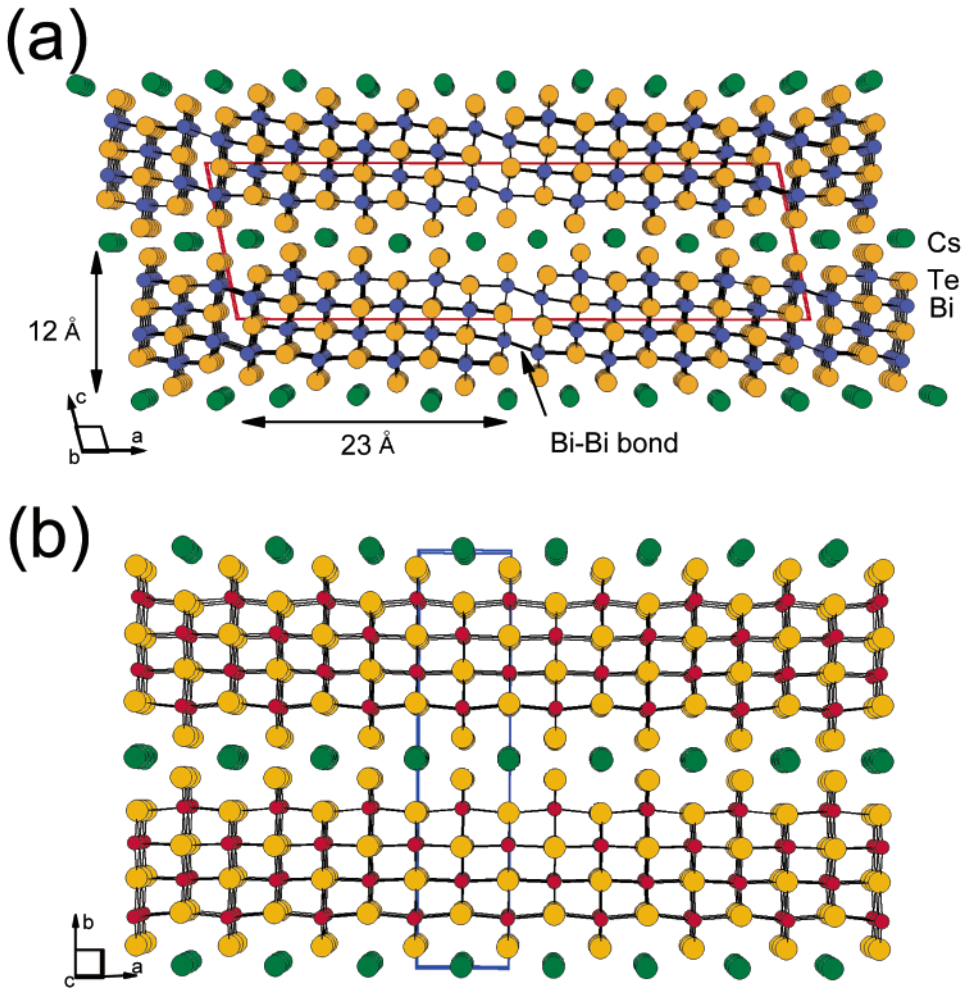

Figure 1. Perspective view of the structures of (a) $CsBi_4Te_6$ along the *b*-axis. Bi atoms are blue; Te atoms are yellow. (b) $CsPbBi_3Te_6$ composed of NaCl-type layers. The red atoms are Bi or Pb atoms (mixed occupancy). In $CsBi_4Te_6$, the $[Bi_4Te_6]$ slabs have a finite width, with 12 × 23 Å^2 cross-section area, are interconnected side by side, and are linked by Bi−Bi bonds at 3.238(1) Å. In $CsPbBi_3Te_6$, the slabs have infinite width and extend continuously along the crystallographic *a*-axis.

tion of Cs metal with Bi_2Te_3. For example, melting the mixture of Cs metal[32] and Bi_2Te_3 with a torch flame produces quantitatively a pure polycrystalline ingot of $CsBi_4Te_6$ in a very short period. Alternatively, the slow vapor transport of Cs metal to Bi_2Te_3 is also successful and forms well-oriented $CsBi_4Te_6$ ingots with good reproducibility. The compound $CsBi_4Te_6$ has a characteristic needlelike morphology and good stability in air and water.

DTA performed on $CsBi_4Te_6$ showed that the compound melts at 545 °C.[33] Molten $CsBi_4Te_6$ can be susceptible to evaporative Cs loss, giving rise to some Bi_2Te_3. Therefore, a successful recrystallization from the melt must take into account the vapor pressure. The Raman spectrum of $CsBi_4Te_6$ crystals shows three Bi−Te vibration modes at 111, 133, and 181 cm^{-1} that are also consistently observed in Bi_2Te_3.

Structure Description. $CsBi_4Te_6$ crystallizes in the space group *C*2/*m* and presents a new type of layered structure composed of anionic infinitely long $[Bi_4Te_6]^-$ blocks and Cs^+ ions residing in the interlayer space, see Figure 1a. The $[Bi_4Te_6]^-$ block can be regarded as an excised fragment out of the NaCl latttice. This block is two Bi octahedra thick and four Bi octahedra wide (12 × 23 Å^2) in the *ac*-plane and infinitely long in the *b*-direction, thus having the shape of an infinite rod that has a rectangular cross section. We emphasize, therefore, that these slabs are strongly anisotropic to the point that the structure is in essence one-dimensional, and this is consistent with the characteristic needlelike morphology of the crystals, see Figure 2. The cleavage of these crystals is strongly preferred along the *ab*-plane which is the plane accommodating the Cs layers.

Bi_2Te_3- and NaCl-type Bi/Q (Q = Te, Se, S) structural units are the archetypical building blocks of group 15 metal chalcogenides.[4b] These blocks are combined in a variety of different fashions and different sizes to build unique structures, as in α-, β-$K_2Bi_8Q_{13}$ (Q = S,[13] Se[6,14]), $K_{2.5}Bi_{8.5}Se_{14}$,[6] $KBi_{6.33}S_{10}$,[13] and $KM_4Bi_7Se_{15}$ (M = Sn, Pb).[16] In $CsBi_4Te_6$, however, the Bi/Te layers consist of only NaCl-type Bi/Te blocks in which inner Bi atoms are coordinated to six Te atoms in a slightly distorted octahedral geometry with distances ranging from 2.974(1) to 3.403(1) Å, see Tables 3 and 4. Interestingly, this preference of structure type for the Bi/Te building block is also

(32) Because of difficulty in handling the exact amount of Cs metal, a slight excess (≤3%) of Cs metal was used in all reactions.
(33) A loss of Cs metal may take place in differential thermal analysis due to the reaction of $CsBi_4Te_6$ with a silica container. With the use of a normal furnace and a graphite container in which any side reaction can be avoided, however, congruent melting of $CsBi_4Te_6$ was confirmed by XRD after a melting/recrystallization cycle.

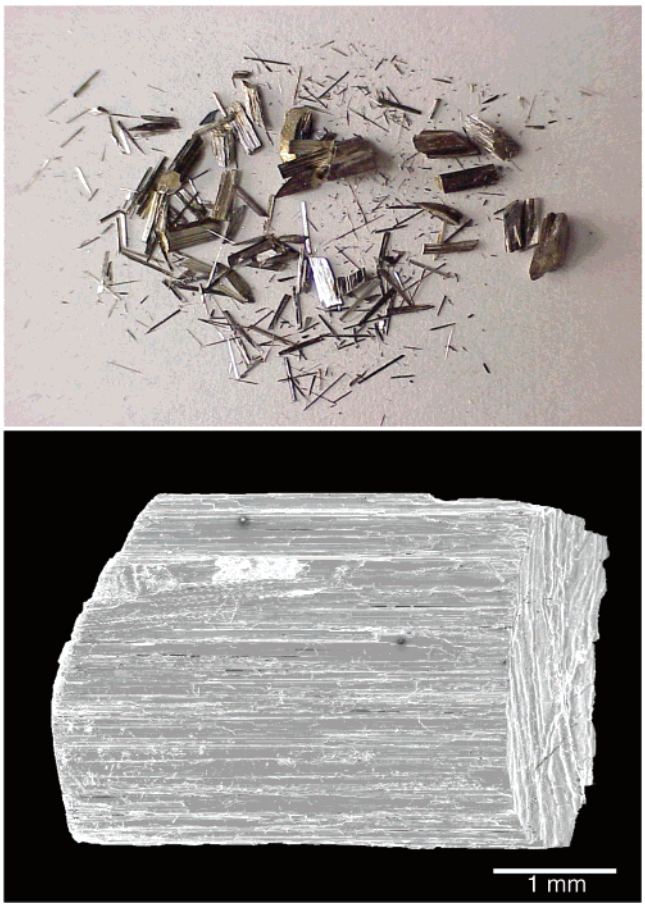

Figure 2. The crystals (top) and oriented ingot (bottom) of $CsBi_4Te_6$. The direction of crystal growth is the *b*-axis in the structure.

Table 3. Selected Bond Distances (Å) in $CsBi_4Te_6$ with Standard Deviations in Parentheses

Bi(1)−Te(1) × 2	3.3713(11)	Bi(6)−Te(7)	3.3092(14)
Bi(1)−Te(2)	3.0538(14)	Bi(6)−Te(7)	3.3087(14)
Bi(1)−Te(3)	2.9956(10)	Bi(6)−Te(8) × 2	2.9981(11)
Bi(1)−Te(3)	2.9957(10)	Bi(6)−Te(10)	2.9740(14)
Bi(1)−Te(4)	3.4031(14)	Bi(7)−Te(2)	3.3835(14)
Bi(2)−Te(1)	3.1229(14)	Bi(7)−Te(11) × 2	3.0362(11)
Bi(2)−Te(4) × 2	3.1180(11)	Bi(7)−Te(12) × 2	3.3334(12)
Bi(2)−Te(5)	3.2205(14)	Bi(7)−Bi(8)	3.2383(10)
Bi(2)−Te(5) × 2	3.2263(11)	Bi(8)−Te(10) × 2	3.0558(11)
Bi(3)−Te(1) × 2	3.2099(11)	Bi(8)−Te(12) × 2	3.3231(12)
Bi(3)−Te(5)	3.2798(13)	Cs(1)−Te(2)	3.956(2)
Bi(3)−Te(6)	3.0640(14)	Cs(1)−Te(3) × 2	4.182(2)
Bi(3)−Te(7) × 2	3.0830(11)	Cs(1)−Te(8)	4.047(2)
Bi(4)−Te(1)	3.3920(14)	Cs(1)−Te(10) × 2	4.003(2)
Bi(4)−Te(2) × 2	3.0925(11)	Cs(1)−Te(11) × 2	4.137(2)
Bi(4)−Te(6) × 2	3.2161(11)	Cs(1)−Te(11) × 2	4.029(2)
Bi(4)−Te(12)	3.0178(14)	Cs(2)−Te(3)	3.842(2)
Bi(5)−Te(4)	3.3033(14)	Cs(2)−Te(4) × 2	4.060(2)
Bi(5)−Te(4)	3.3027(14)	Cs(2)−Bi(6)	4.570(2)
Bi(5)−Te(5) × 2	3.4024(11)	Cs(2)−Te(7)	3.892(2)
Bi(5)−Te(7)	3.0604(14)	Cs(2)−Te(8) × 2	3.973(2)
Bi(5)−Te(9) × 2	3.0012(11)	Cs(2)−Te(9)	3.761(2)
Bi(6)−Te(6) × 2	3.3538(11)	Cs(2)−Te(9) × 2	4.104(2)

shown in other bismuth telluride compounds containing Rb and Cs. For example, $Rb_{0.5}Bi_{1.83}Te_3$,[34] $AMBi_3Te_6$, and $AM_2Bi_3Te_7$ (A = Rb, Cs; M = Sn, Pb)[34] consist of similar NaCl-type Bi/Te layers but of infinite width, see Figure 1b. This is probably due to the size effect of alkali metal versus Bi/Q block; that is, large alkali cations, Rb and Cs, fit better in NaCl-type blocks than in Bi_2Te_3-type blocks, providing a smaller interlayer space for alkali metals.[35]

Table 4. Selected Bond Angles (deg) in $CsBi_4Te_6$ with Standard Deviations in Parentheses

Te(1)−Bi(1)−Te(1)	81.53(3)	Te(12)−Bi(4)−Te(1)	175.66(4)
Te(1)−Bi(1)−Te(4)	82.51(3)	Te(4)−Bi(5)−Te(5)	87.32(3)
Te(2)−Bi(1)−Te(1)	89.48(3)	Te(5)−Bi(5)−Te(5)	80.63(3)
Te(3)−Bi(1)−Te(1)	91.94(2)	Te(7)−Bi(5)−Te(5)	86.57(3)
Te(3)−Bi(1)−Te(2)	90.59(3)	Te(9)−Bi(5)−Te(4)	96.24(3)
Te(3)−Bi(1)−Te(3)	94.58(4)	Te(9)−Bi(5)−Te(5)	92.36(2)
Te(3)−Bi(1)−Te(4)	96.58(3)	Te(9)−Bi(5)−Te(7)	89.19(3)
Te(3)−Bi(1)−Te(1)	173.47(3)	Te(9)−Bi(5)−Te(9)	94.35(4)
Te(2)−Bi(1)−Te(4)	169.41(4)	Te(7)−Bi(5)−Te(4)	171.99(4)
Te(1)−Bi(2)−Te(5)	89.99(3)	Te(9)−Bi(5)−Te(5)	172.01(3)
Te(4)−Bi(2)−Te(1)	91.41(3)	Te(6)−Bi(6)−Te(6)	82.04(3)
Te(4)−Bi(2)−Te(4)	89.82(4)	Te(7)−Bi(6)−Te(6)	83.80(3)
Te(4)−Bi(2)−Te(5)	93.83(3)	Te(8)−Bi(6)−Te(6)	91.73(2)
Te(4)−Bi(2)−Te(5)	92.05(2)	Te(8)−Bi(6)−Te(7)	94.93(3)
Te(5)−Bi(2)−Te(5)	86.05(4)	Te(8)−Bi(6)−Te(8)	94.48(4)
Te(5)−Bi(2)−Te(5)	84.61(3)	Te(10)−Bi(6)−Te(6)	90.22(3)
Te(1)−Bi(2)−Te(5)	172.60(4)	Te(10)−Bi(6)−Te(8)	90.45(3)
Te(4)−Bi(2)−Te(5)	177.64(3)	Te(8)−Bi(6)−Te(6)	173.74(3)
Te(1)−Bi(3)−Te(1)	86.59(4)	Te(10)−Bi(6)−Te(7)	172.07(5)
Te(1)−Bi(3)−Te(5)	87.55(3)	Bi(8)−Bi(7)−Te(12)	82.14(3)
Te(6)−Bi(3)−Te(1)	91.25(3)	Te(11)−Bi(7)−Te(2)	88.74(3)
Te(6)−Bi(3)−Te(7)	92.75(3)	Te(11)−Bi(7)−Bi(8)	103.93(3)
Te(7)−Bi(3)−Te(1)	91.00(2)	Te(11)−Bi(7)−Te(11)	92.94(4)
Te(7)−Bi(3)−Te(5)	88.40(3)	Te(11)−Bi(7)−Te(12)	91.76(2)
Te(7)−Bi(3)−Te(7)	91.12(4)	Te(12)−Bi(7)−Te(2)	83.90(3)
Te(6)−Bi(3)−Te(5)	178.35(4)	Te(12)−Bi(7)−Te(12)	82.65(4)
Te(7)−Bi(3)−Te(1)	175.37(4)	Bi(8)−Bi(7)−Te(2)	161.37(4)
Te(2)−Bi(4)−Te(1)	88.47(3)	Te(11)−Bi(7)−Te(12)	171.18(4)
Te(2)−Bi(4)−Te(2)	90.77(4)	Bi(7)−Bi(8)−Te(12)	106.45(3)
Te(2)−Bi(4)−Te(6)	91.11(2)	Te(10)−Bi(8)−Bi(7)	86.27(3)
Te(6)−Bi(4)−Te(1)	85.46(3)	Te(10)−Bi(8)−Te(10)	92.17(4)
Te(6)−Bi(4)−Te(6)	86.38(4)	Te(10)−Bi(8)−Te(12)	91.16(2)
Te(12)−Bi(4)−Te(2)	94.57(3)	Te(12)−Bi(8)−Te(12)	82.97(4)
Te(12)−Bi(4)−Te(6)	91.39(3)	Te(10)−Bi(8)−Te(12)	167.05(4)
Te(2)−Bi(4)−Te(6)	173.60(4)		

$CsBi_4Te_6$ can be regarded as a reduced version of Bi_2Te_3. Apparently, the addition of one electron per 2 equiv of Bi_2Te_3 does not give a formal intercalation compound (e.g., $Cs_xBi_2Te_3$), but causes a rather dramatic reorganization of the Bi_2Te_3 framework and reveals an inability to delocalize such electrons. The added electrons then localize on Bi atoms, giving formally Bi^{2+} (rare in Bi chemistry) and Bi−Bi bonds of 3.2383(10) Å. These unusual bonds "stitch" the $[Bi_4Te_6]$ slabs together. The Bi−Bi distance in $CsBi_4Te_6$ is comparable to a Bi−Bi distance of 3.267(6) Å in BiTe,[36] a metallic compound possessing a layer of Bi atoms inserted between Bi_2Te_3 layers. Interestingly, isolated Bi−Bi bonds in solids are a rare occurrence. The other example of such a functionality we are aware of is in $Bi_2Ga_2Q_8$ (Q = S, Se), where the relevant distance is 3.148 Å.[37]

The anionic $[Bi_4Te_6]$ slabs in $CsBi_4Te_6$ are separated by layers of Cs^+ cations, which are in two different coordination environments. The Cs(1) ions are located at the corner of each $[Bi_4Te_6]$ slab and coordinated by 10 peripherally distributed Te

(34) (a) Hsu, K.-F.; Lal, S.; Hogan, T.; Kanatzidis, M. G. *Chem. Commun.* **2002**, *13*, 1380−1381. (b) Hsu, K.-F.; Chung, D.-Y.; Lal, S.; Mrotzek, A.; Kyratsi, T.; Hogan, T.; Kanatzidis, M. G. *J. Am. Chem. Soc.* **2002**, *124*, 2410−2411. (c) Hsu, K.-F.; Chung, D.-Y.; Lal, S.; Hogan, T.; Kanatzidis, M. G. *Mater. Res. Soc. Symp. Proc.* **2002**, G8.25.

(35) This behavior is also found in selenide compounds, $A_2Bi_8Se_{13}$ (A = Rb, Cs), which contain only NaCl-type Bi/Se blocks connected by short CdI_2-type fragments: Iordanidis, L.; Brazis, P. W.; Kyratsi, T.; Ireland, J.; Lane, M.; Kannewurf, C. R.; Chen, W.; Dyck, J. S.; Uher, C.; Ghelani, N. A.; Hogan, T.; Kanatzidis, M. G. *Chem. Mater.* **2001**, *13*, *622*.

(36) Kazuo, Y.; Kuniaki, K.; Takeo, M. *Acta Crystallogr.* **1979**, *B35*, 147−149.

(37) Kalpen, H.; Hoenle, W.; Somer, M.; Schwartz, U.; Peters, K.; von Schnering, H. G.; Blachnik, R. *Z. Anorg. Allg. Chem.* **1998**, *624*, 1137.

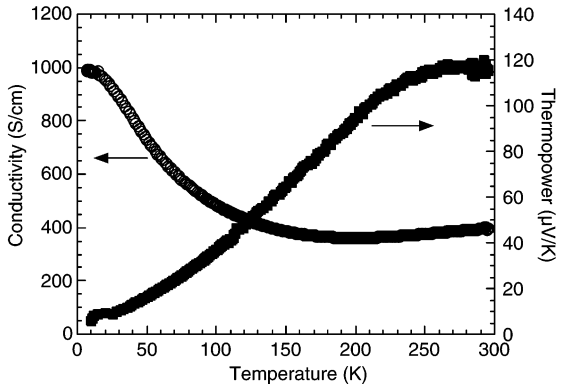

Figure 3. Typical electrical conductivity and thermopower for a single-crystal sample of as-prepared $CsBi_4Te_6$ as a function of temperature. The measurements were carried out along the needle direction.

atoms. The Cs(2) ions are located between the $[Bi_4Te_6]$ slabs and coordinated by nine terminal Te atoms. The average Cs−Te distance is 4.025 Å. The thermal displacement parameters of Cs atoms are about 1.6 times greater than those of Bi and Te atoms, suggesting that Cs atoms may be playing the role of rattlers. If Cs atoms are dynamically rattling in the cages, they will help to reduce the lattice thermal conductivity of $CsBi_4Te_6$ by scattering heat-carrying acoustic phonons.[38] However, the possibility of static disorder of Cs atoms, which are also represented by relatively high thermal displacement parameters, cannot be excluded in this case.

Electronic, Charge-Transport, and Thermoelectric Properties. Undoped "As-Prepared" $CsBi_4Te_6$. Before we describe the dependence of electronic and thermoelectric properties of $CsBi_4Te_6$ as a function for doping, we need to characterize the properties of the so-called "as-prepared" material, which is material obtained from a preparative reaction without any intentional attempt to dope it. Of course, there is no such entity as undoped (i.e., intrinsic semiconductor) material, as it is impossible to prepare samples free of impurities. Several crystals of each sample batch were examined to check how reproducible the transport properties were among the crystals of different batches. There is a large variation in the properties of the "as-prepared" crystals representing different degrees of doping due to adventitious impurities. The room-temperature conductivity and thermopower for single crystals of "as-prepared" $CsBi_4Te_6$ are in the range of 900−450 S/cm and 90−150 μV/K, respectively, see Figure 3. These samples were invariably p-type, indicating holes as the majority carrier. The conductivity and thermopower data of $CsBi_4Te_6$ follow typical behavior of a degenerate narrow gap semiconductor. The conductivity exhibits a weak negative temperature dependence, and the thermopower exhibits a positive temperature dependence and large values. By comparison, at room temperature the unoptimized Bi_2Te_3 has similar properties with 450−1500 S/cm and 80−150 μV/K, whereas optimized $Bi_{2-x}Sb_xTe_{3-y}Se_y$ samples, exhibiting ZT $\approx$ 1 and used in thermoelectric devices, show ∼800−1000 S/cm and ∼±220 μV/K. The rather similar magnitudes of conductivity and thermopower of $CsBi_4Te_6$ as compared to those of Bi_2Te_3 and the ability to dramatically optimize the thermoelectric properties of Bi_2Te_3 via doping encouraged us to pursue systematic exploratory doping studies on $CsBi_4Te_6$ as presented below.

Optimization through Doping: p-type $CsBi_4Te_6$. In general, the charge-transport properties of narrow gap semiconductors are sensitive to extremely small changes in effective mass, mobility, and concentration of carriers around the Fermi level. To probe the ability of $CsBi_4Te_6$ to change its electrical properties by changing these parameters, we added various extrinsic dopants into the reaction mixture in anticipation that they will end up in the structure and will either donate holes or electrons to the system. Our aim was to learn how this new material is doped by various chemical agents and to be able to create and control p-type and n-type samples with the ultimate goal of maximizing the thermoelectric figure of merit ZT. This optimization process is necessary to achieve suitability for a practical thermoelectric device.

The doping of $CsBi_4Te_6$ was done with various chemical "impurities" such as SbI_3, BiI_3, CuCl, SnTe, In_2Te_3, Sb, Bi, Sn, Zn, Mg, Te, Ge, Pt, and Pr in amounts ranging from 0.02 to 4.0 mol %. The rationale behind the choice of these particular agents varied. In most cases, we chose the dopants to achieve a change in carrier concentration or the type of majority carrier (e.g., substitution of Sb for Te or Te for Bi is expected to create a hole or an electron carrier, respectively). In several other cases, the dopants were chosen almost randomly and in an exploratory fashion (e.g., Mg, Pt, Zn) to probe how they acted when introduced in the structure. The doping studies showed clearly that the charge-transport properties of $CsBi_4Te_6$ greatly rely on both the type and the percent of the doping agent. To evaluate the effectiveness of each dopant, the power factor ($S^2\sigma$) of the doped material was calculated from the conductivity and thermopower data as a function of temperature. These power factor data are also necessary to determine the temperature (at the maximum $S^2\sigma$) of the highest thermoelectric efficiency as well as the optimal doping level for each dopant, see Table 5.

SnTe was examined to substitute Bi atoms with Sn atoms and generate more carriers. This was expected to increase the conductivity and decrease the thermopower with increasing SnTe. Indeed, from an average value of 363 S/cm for the undoped material at room temperature, SnTe doping in the range of 0.3−1.5% gradually increased the conductivity from 899 to 2584 S/cm and decreased the thermopower from 103 to 54 μV/K (room-temperature values).

SbI_3 and BiI_3 were chosen with the purpose of placing iodine atoms on the Te sites. Surprisingly, the materials were consistently p-doped rather than n-doped over the range of doping level we applied. The most promising material was 0.05 mol % SbI_3-doped $CsBi_4Te_6$, having a maximum power factor of ∼51.5 $\mu W/cm\cdot K^2$ at 184 K where the values of conductivity and thermopower reach ∼1927 S/cm and ∼163 μV/K respectively, see Table 5 and Figure 4. Power factors for each doped $CsBi_4Te_6$ sample giving noticeably high values are shown as a function of temperature in Figure 5. It is also interesting to compare the maximum power factor of the doped $CsBi_4Te_6$ to that of a commercial p-type $Bi_{2-x}Sb_xTe_3$ alloy. The maximum value for a p-type $Bi_{2-x}Sb_xTe_3$ sample is ∼42.5 $\mu W/cm\cdot K^2$ at ∼225 K, which is below the corresponding values for all 0.05% SbI_3-doped samples examined. It is significant to point out that the maximum in power factor occurs at ∼184 K, which is 70−

(38) (a) Slack, G. A. In *CRC Handbook of Thermoelectrics*; Rowe, D. M., Ed.; CRC Press: Boca Raton, FL, 1995; Chapter 34, p 407. (b) Slack, B. C.; Chakoumakos, B. C.; Mandrus, D.; Sharp, J. W. *J. Solid State Chem.* **1999**, *146*, 528−532.

Table 5. Power Factor Values for Each Dopant at Room Temperature and the Temperature Where the Maximum Value Occurs, and Electrical Conductivity and Thermopower Values Giving Rise to the Maximum Power Factor

dopant	concentration mol %	$S^2\sigma$ (295 K) μW/cm·K^2	max $S^2\sigma$ μW/cm·K^2	σ^a (max $S^2\sigma$) S/cm	S^a (max $S^2\sigma$) μV/K	temp^a (max $S^2\sigma$) K
p-Bi_2Te_3[b]		39.9	42.5			225
undoped		4.8	6.4			211
SbI_3	0.02	26.7	28.8	1283	150	235
	0.05	34.0	51.5	1927	163	184
	0.1	11.0	22.1	1197	136	165
	0.2	9.0	13.9	1107	112	214
	0.3	5.0	7.1	569	112	166
	0.4	6.3	7.2	864	91	248
BiI_3	0.1	7.6	8.8	852	102	235
	0.2	11.2	11.5	1193	98	270
	0.3	14.5	45.0	4870	96	147
	0.4	3.0	3.0	960	55	295
CuCl	0.02	8.0	8.9	883	101	250
	0.05	11.1	15.1	1579	98	181
	0.1	6.6	6.7	845	89	274
	0.5	7.3	8.1	904	94	225
SnTe	0.3	9.5	11.9	1313	95	229
	0.6	7.8	7.9	1379	76	272
	1.0	4.9	5.1	1734	65	258
	1.5	3.4	3.5	3176	50	282
Sn	0.2	1.3	1.3	836	39	295
	0.5	0.4	21.9	5499	−63	127
	1.0	0.02	7.4	1292	−76	139
	2.0	0.08	4.6	3130	−39	131
In_2Te_3	0.3	1.6	1.6	655	49	295
	0.6	3.2	3.2	839	62	295
	0.9	13.8	17.0	1821	97	214
	1.5	16.2	30.6	2778	104	159
	3.0	0.03	9.6	1175	−90	136
	4.0	1.7	3.4	1558	−47	111
Bi	0.02	6.8	6.9	820	92	290
	0.06	6.0	9.4	731	114	212
	0.1	15.7	40.9	1170	187	171
	0.2	10.5	32.3	1607	142	217
	0.3	4.4	4.9	815	77	253
Sb	0.02	8.1	16.9	1846	96	161
	0.06	16.0	59.8	4562	115	151
	0.1	13.5	39.0	3846	101	109
	0.2	16.8	20.4	1093	136	224
	0.3	29.6	56.2	4550	111	190
Zn	0.3	0.03	16.7	3335	−71	156
	0.5	21.3	23.2	978	154	266
	1.0	5.0	6.2	1987	56	242
Mg	0.1	1.8	1.8	1463	35	295
	0.3	2.1	8.0	2348	−58	107
Te	1.0	0.5	23.8	2709	−94	123

[a] p-type Bi_2Te_3 samples and data obtained from Marlow Industries, Inc., Dallas, Texas. [b] Schindler, J. L.; Hogan, T. P.; Brazis, P. W.; Kannewurf, C. R.; Chung, D.-Y.; Kanatzidis, M. G. *Mater. Res. Soc. Symp. Proc.* **1997**, *478*, 327−332.

100 K lower than that of the best $Bi_{2-x}Sb_xTe_3$ alloys. The latter show maxima in the range 250−300 K depending on doping. Therefore, it is clear that the $CsBi_4Te_6$ system surpasses the performance of $Bi_{2-x}Sb_xTe_3$ alloys when the temperature falls below ∼250 K, establishing the cesium compound as a new low-temperature thermoelectric p-type material. Clearly, this is encouraging and opens possibilities for the realization of new low-temperature thermoelectric devices.

The temperature of the power factor maximum in $CsBi_4Te_6$ can be shifted up or down depending on the nature of the dopant. Of particular interest is the ability to push the temperature maximum even lower. In this respect, the use of BiI_3 as dopant gives even more exciting results than SbI_3. We observed that 0.3% BiI_3 doping resulted in a power factor maximum of ∼45.0 μW/cm·K^2 at ∼147 K, see Figure 5e. This is a record low temperature for a p-type thermoelectric compound, suggesting that a variety of cooling applications may be possible in a relatively wide range of temperatures with $CsBi_4Te_6$.

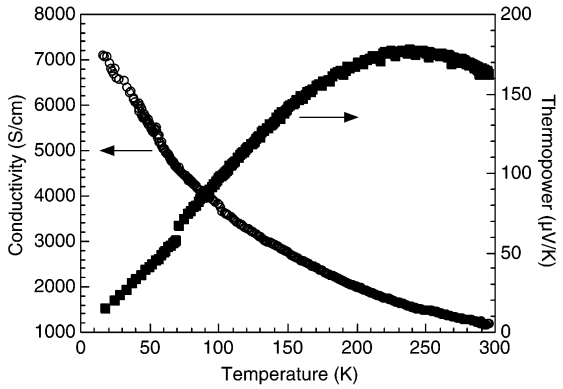

Figure 4. Variable-temperature electrical conductivity and thermopower for a single crystal of 0.05% SbI_3-doped $CsBi_4Te_6$.

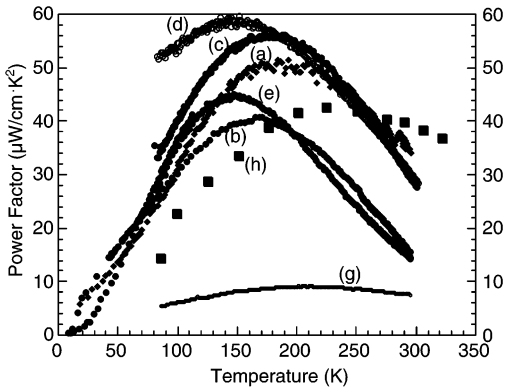

Figure 5. Power factors as a function of temperature for a $CsBi_4Te_6$ sample doped with (a) 0.05% SbI_3, (b) 0.1% Bi, (c) 0.3% Sb, (d) 0.06% Sb, and (e) 0.3% BiI_3. For comparison, the power factor data of (g) an "as-prepared" $CsBi_4Te_6$ sample and (h) commercial p-type doped $Bi_{2-x}Sb_xTe_3$ are shown.

The results from SbI_3 and BiI_3 doping are not consistent with iodine atoms occupying Te sites but instead are in agreement with what would be expected if Sb or Bi atoms were replacing Te atoms. The Sb and Bi atoms having only five valence electrons would introduce a hole in the valence Te-based band in which each Te atom brings six electrons. The fate of I^- is not clear. We surmise that it may not even be incorporated in the compound having phase separated as trace CsI. Based on this assumption, iodine is not necessary and elemental dopants of Sb and Bi should and do reproduce the high power factors. The obtained power factors from Sb and Bi doping are about 40−60 μW/cm·K^2, similar to those obtained for the best SbI_3- and BiI_3-doped materials. 0.1% Bi-doped $CsBi_4Te_6$ shows a significant improvement in thermopower, of which the maximum is 198 μV/K at 224 K. This is the highest value $CsBi_4Te_6$ has ever shown, and the maximum power factor of 40.9 μW/cm·K^2 occurs at 171 K, Figures 5b and 6a. Like 0.05% SbI_3-doped $CsBi_4Te_6$, 0.06% Sb doping also shows a very high power factor which reaches the highest value, 59.8 μW/cm·K^2, at 151 K, Figures 5d and 6b. These high power factors are attributed to high thermopower in Bi doping and to high conductivity in Sb doping. The temperatures at maximum power factor in these two cases are also lower than 184 K for 0.05% SbI_3-doped $CsBi_4Te_6$.

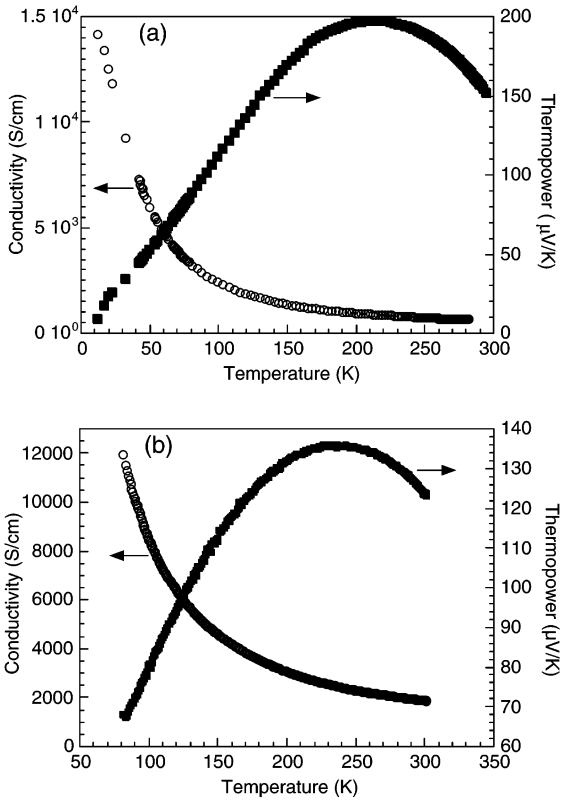

Figure 6. Variable-temperature electrical conductivity and thermopower for single crystals of (a) 0.1% Bi-doped and (b) 0.06% Sb-doped $CsBi_4Te_6$.

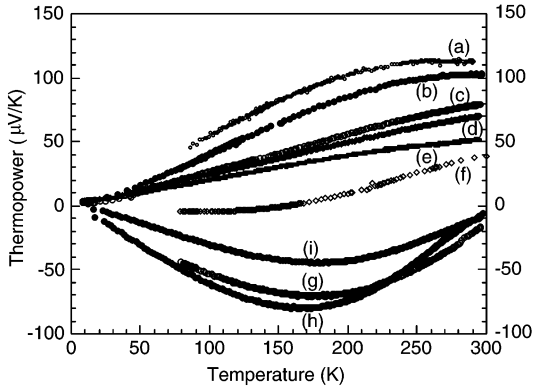

Figure 7. Variable-temperature thermopower data for single crystals of "as-prepared" and doped $CsBi_4Te_6$: (a) "as-prepared", (b) 0.3% SnTe, (c) 0.6% SnTe, (d) 1.0% SnTe, (e) 1.5% SnTe, (f) 0.2% Sn, (g) 0.5% Sn, (h) 1.0% Sn, and (i) 2.0% Sn.

n-type $CsBi_4Te_6$. Following the optimization of p-type samples of $CsBi_4Te_6$, we became interested in n-type materials and their ability to be optimized to a high ZT. Given that iodide doping in the form of SbI_3 and BiI_3 did not give the n-type sample, we carried out a broad search for dopants. We found that Sn, Mg, Zn, Ge, Pr, In_2Te_3, and excess Te result in n-type conductivity. We believe that in the case of In_2Te_3 and Te the n-type behavior originates from Te atom substitution on Bi sites in the structure. It is not clear why the elemental dopants Sn, Mg, Zn, Ge, and Pr gave n-type samples.

Sn doping above the 0.5% level turned the type of charge transport to n-type, see Figure 7. This is consistent with the results presented above that increasing SnTe doping decreased the thermopower, annihilating the p-type carriers. The n-type

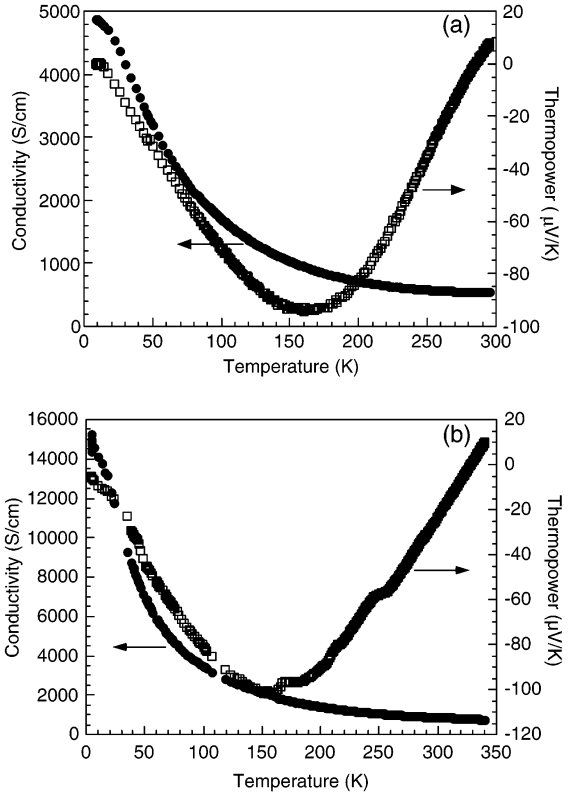

Figure 8. Variable-temperature electrical conductivity and thermopower for a single crystal of (a) 3.0% In_2Te_3-doped and (b) 1.0% Te-doped $CsBi_4Te_6$.

behavior appears, that beyond a certain concentration level of Sn the number of electrons exceeds that of holes. One mechanism for generating electron carriers is through Sn atom substitution of Bi atom in the structure. Sn doping does not show a clear systematic dependence upon the doping level as observed in SnTe doping. The room-temperature conductivity is in the range from 560 S/cm for 1.0% Sn doping to 1655 S/cm for 0.5% Sn doping.

Doping with In_2Te_3 has been known to produce a weak donor effect in Bi_2Te_3.[39] Likewise, $CsBi_4Te_6$ doped with In_2Te_3 exhibits n-type behavior at high concentration of In_2Te_3, see Figure 8a. The maximum negative thermopower of -95 μV/K was observed at 160 K from a 3.0% doped sample, see Figure 9A.

When $CsBi_4Te_6$ was synthesized with a slight excess of Te, n-type material was obtained probably because excess Te atoms occupy Bi sites. The maximum thermopower value of -95 μV/K was observed at 160 K in 1.0% Te-doped material, see Figure 8b.

The elemental dopants, Zn and Mg, provided n-type conductivity perhaps due to their small size that allows them to be placed in interstitial spaces of the structure releasing two electrons per atom. The type and concentration of the majority carrier significantly depend on the doping level of Zn and Mg, see Figure 9B.

Another interesting way to produce n-type material is to anneal p-type $CsBi_4Te_6$ at 250 °C. For example, an annealed sample of p-type $CsBi_4Te_6$ at 250 °C for over 2 h under vacuum

(39) Chizhevskaya, S. N.; Shelimova, L. E. *Inorg. Mater.* **1995**, *31*, 1083−1095.

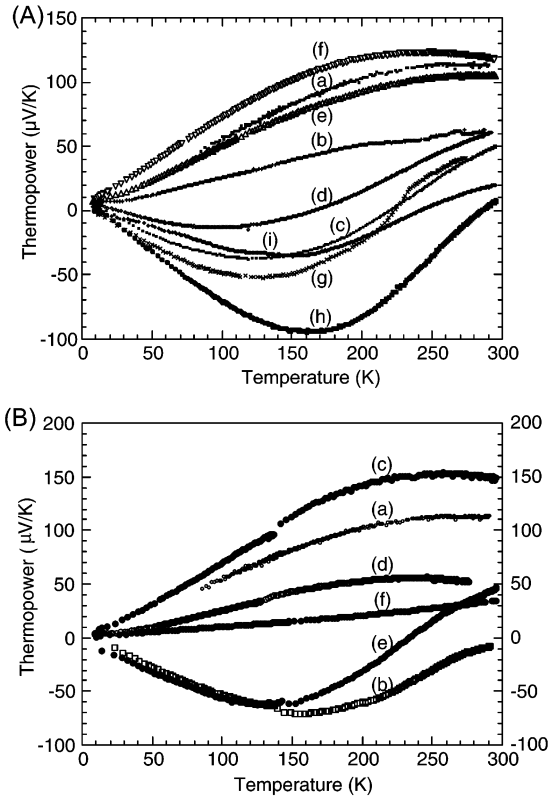

Figure 9. Variable-temperature thermopower data for single crystals of (a) "as-prepared" $CsBi_4Te_6$ and (A) In_2Te_3-doped with (b) 0.15%, (c) 0.3%, (d) 0.6%, (e) 0.9%, (f) 1.5%, (g) 2.0%, (h) 3.0%, and (i) 4.0% and (B) doped with (b) 0.3% Zn, (c) 0.5% Zn, (d) 1.0% Zn, (e) 0.1% Mg, and (f) 0.3% Mg.

turned out to be an n-type material with a maximum thermopower of -93 μV/K at 220 K (-74 μV/K at room temperature). The reason for this p- to n-type conversion is probably due to the fact that a loss of Te atoms in Bi/Te layers under vacuum at an elevated temperature could provide additional electrons.[40]

It is very encouraging that $CsBi_4Te_6$ is subject to considerable doping manipulation, much like Bi_2Te_3, and to production of both p- and n-type materials which are necessary to build thermoelectric devices. For the p-type materials, which $CsBi_4Te_6$ tends most likely to be (see the Electronic Band Structure section), maximum power factors of 51.5, 59.8, 45.0, and 40.9 μW/cm·K^2 were measured at 184, 151, 147, and 171 K, respectively, by 0.05% SbI_3, 0.06% Sb, 0.3% BiI_3, and 0.1% Bi doping. From these results, Bi and Sb appear to be very effective p-type dopants. In contrast, n-type doping on $CsBi_4Te_6$ was achieved with only a few doping agents in relatively high doping concentrations, see Table 5. The highest power factors were obtained by 0.5% Sn and 1.0% Te doping with 21.9 and 23.8 μW/cm·K^2 at the temperatures of 127 and 123 K, respectively, see Figure 10. Therefore, sophisticated chemical manipulations are needed to further improve the power factor not only for n-type $CsBi_4Te_6$ but also for p-type. Although doping $CsBi_4Te_6$ with the above reagents apparently occurs, it is not clear yet which sites in the crystal structure are being affected by each dopant.

(40) Chen, B. X.; Uher, C.; Iordanidis, L.; Kanatzidis, M. G. *Chem. Mater.* **1997**, *9*, 1655−1658.

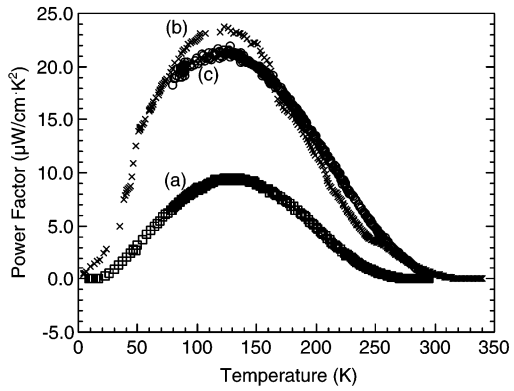

Figure 10. Power factors as a function of temperature for an n-type $CsBi_4Te_6$ sample doped with (a) 3.0% In_2Te_3, (b) 1.0% Te, and (c) 0.5% Sn.

Figure 11 presents ZT versus temperature of a number of high-performing TE materials; as shown, several exceed ZT = 1 at high temperatures (>600 K). However, below room temperature, except for $Bi_{2-x}Sb_xTe_{3-y}Se_y$, almost no materials with high ZT have been reported. In this figure, it should be noted that the superlattice Bi_2Te_3/Sb_2Te_3[41] showing ZT $\approx$ 1.7−2.6 is a thin film material synthesized by a considerably different technique from that for the bulk materials such as $CsBi_4Te_6$, and it may only be utilized in microscale thermoelectric applications.

$CsBi_4Te_6$ shows a very wide temperature range, giving high values (>30 μW/cm·K^2) of power factor by different doping, from 109 K (39.0 μW/cm·K^2 by 0.1% Sb) to 217 K (32.3 μW/cm·K^2 by 0.2% Bi) for p-type materials, see Figures 5, 10, and 11 and Table 5. The ability to shift the ZT maximum over a range of 100 K is a positive feature for applications, and it is similar to that of bismuth telluride alloys. The only difference is $CsBi_4Te_6$ is active at lower temperatures. For efficient low-temperature thermoelectric devices using p-type $CsBi_4Te_6$, they can be fabricated as follows: (1) a high ZT n-type thermoelectric material such as the Bi/Sb alloys having a wide working temperature (80−200 K) and (2) possible n-type $CsBi_4Te_6$ materials if future studies succeed in improving ZT to levels comparable to those of the p-type materials.[42]

Carrier Concentration and Mobility in $CsBi_4Te_6$. Hall effect measurements were performed to estimate the concentration and mobility of carriers. The room-temperature carrier concentrations (3×10^{18} to 10^{19} cm^{-3}) measured for the 0.1% and 0.2% SbI_3-doped p-type $CsBi_4Te_6$ samples are only slightly less than the generally accepted optimal value ($\sim 10^{19}$ cm^{-3})[43] for thermoelectric applications, see Figure 12. Carrier concentra-

(41) (a) Venkatasubramanian, R.; Siivola, E.; Colpitts, T.; O'Quinn, B. *Nature* **2001**, *413*, 597−602. (b) $CeFe_{4-x}Co_xSb_{12}$: Fleurial, J. P.; Borshchevsky, A.; Caillat, T.; Morelli, D. T.; Meisner, G. P. In *Proceedings of the 15th International Conference on Thermoelectrics*; Caillat, T., Ed.; IEEE: Piscataway, NJ, 1996; pp 91−95 . (c) TAGS-85: Skrabek, E. A. Compositional Variations of TAGS-type Materials. Presented at the Fourth RTG Working Group Meeting, Daytona Beach, FL, March, 1973. (d) PbTe: Tritt, T. M. *Science* **1999**, *283*, 804−805. (e) SiGe: Vining, C. B. Modern Perspectives on Thermoelectrics and Related Materials. In *Materials Research Society Symposium Proceedings*; Allred, D. D., Vining, C. B., Slack, G. A., Eds.; Materials Research Society: Pittsburgh, PA, 1991; Vol. 234, p 95. (f) Wölfing, B.; Kloc, C.; Teubner, J.; Bucher, E. *Phys. Rev. Lett.* **2001**, *86*, 4350−4353.

(42) Currently, the temperature at maximum power factor for n-type materials is found around 125 K (21.9 μW/cm·K^2 by 0.5% Sn and 23.8 μW/cm·K^2 by 1.0% Te), see Table 5.

(43) (a) Tritt, T. M. *Mater. Res. Soc. Symp. Proc.* **1997**, *478*, 25−35. (b) Wood, C. *Rep. Prog. Phys.* **1991**, *51*, 459−539. (c) Ioffe, A. F. *Semiconductor Thermoelements and Thermoelectric Cooling*; Inforsearch Ltd.: London, 1957.

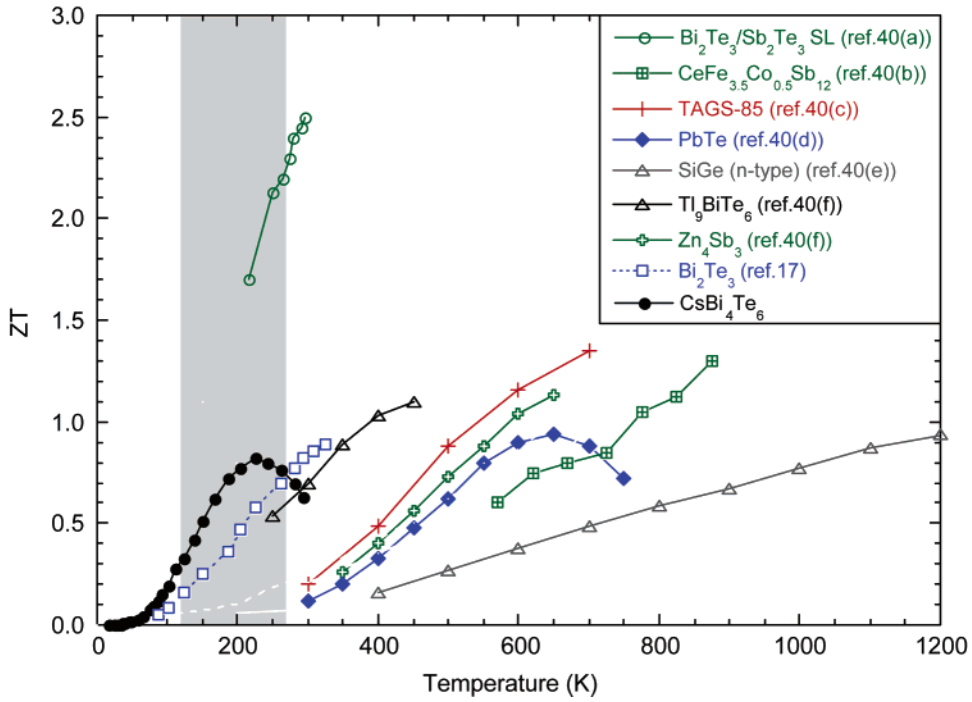

Figure 11. ZT data of the best-known thermoelectric materials as a function of temperature. At the shaded region, $CsBi_4Te_6$ could be possibly available for thermoelectric applications.

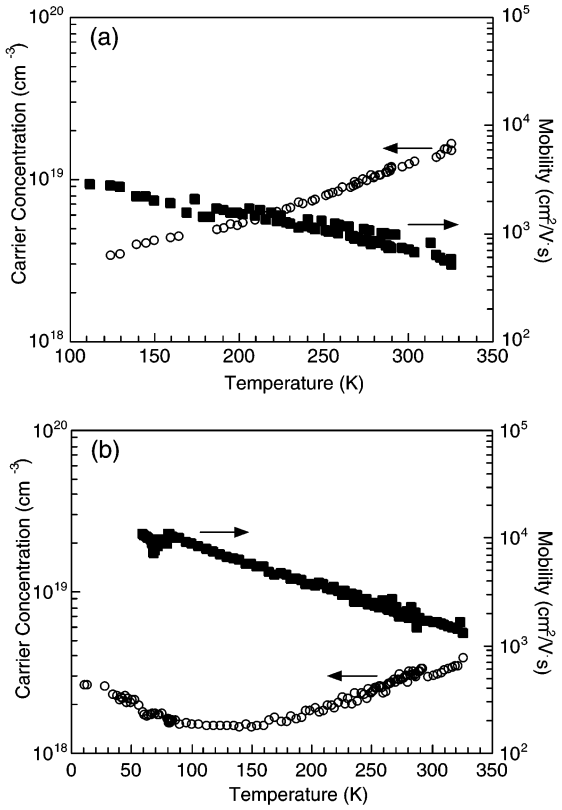

Figure 12. Carrier concentration and hole mobility as a function of temperature for (a) 0.1% SbI_3-doped and (b) 0.2% SbI_3-doped $CsBi_4Te_6$ crystals.

tion was found to be weakly dependent on temperature and doping level, with values decreasing as the temperature was lowered and as the doping increased. For these samples, the carrier concentration data could be correlated with the power factor data, showing that the latter decreased as carrier concentration moved away from 10^{19} cm^{-3}.

Hole mobilities calculated from the electrical conductivity and Hall data show exponentially decreasing mobility as the temperature increases. The hole mobilities in SbI_3-doped $CsBi_4Te_6$ samples range between 700 and 1000 $cm^2/V\cdot s$ at room temperature. These are significantly greater than those typically found in the optimized p-type Bi_2Te_3 alloy (~380 $cm^2/V\cdot s$).[44] At low temperatures, the mobilities rise to >5000 $cm^2/V\cdot s$. The very high hole mobilities could be due to the one-dimensional structure character of $CsBi_4Te_6$ and the lack of atomic disorder in its crystal lattice.

For n-type materials, samples doped with Sn and Te were examined. 0.5% Sn-doped $CsBi_4Te_6$ was selected for Hall measurements on the basis of the maximum power factor of 21.9 $\mu W/cm^2\cdot K$ at 127 K. The carrier concentration varies from 1.2×10^{19} cm^{-3} at 22.4 K to 2.38×10^{19} cm^{-3} at 312 K, Figure 13a. At room temperature, the carrier concentration and mobility were 2.11×10^{19} cm^{-3} and 325 $cm^2/V\cdot s$, respectively. The mobility decreases as the temperature increases, varying from 4600 $cm^2/V\cdot s$ at 22.4 K to 302 $cm^2/V\cdot s$ at 312 K.

For 1.0% Te-doped $CsBi_4Te_6$, the carrier concentration and mobility showed temperature dependence similar to those of 0.5% Sn-doped material, see Figure 13b. The carrier concentration varied from 1.16×10^{19} to 1.48×10^{19} cm^{-3}, and the mobility ranged from 5890 to 419 $cm^2/V\cdot s$ in the temperature range of 27−267 K. The maximum power factor of 21.7 $\mu W/cm^2\cdot K$ occurred at 123 K for this material with the carrier concentration of 1.20×10^{19} cm^{-3} and mobility of 1260 $cm^2/V\cdot s$, both greater than the values of SbI_3-doped p-type materials. It is interesting to note that the maximum power factors achieved with 0.5% Sn- and 1.0% Te-doped materials are similar and occur at about the same low temperature, 127 and 123 K.

Thermal Conductivity and Thermoelectric Performance. Before a ZT estimation can be made for the optimized samples

(44) Süssmann, H.; Heiliger, W. *Proc. Conf. Transport. in Compound Semiconductors*; MLT: Halle, Germany, KTB series, 1982; p 100.

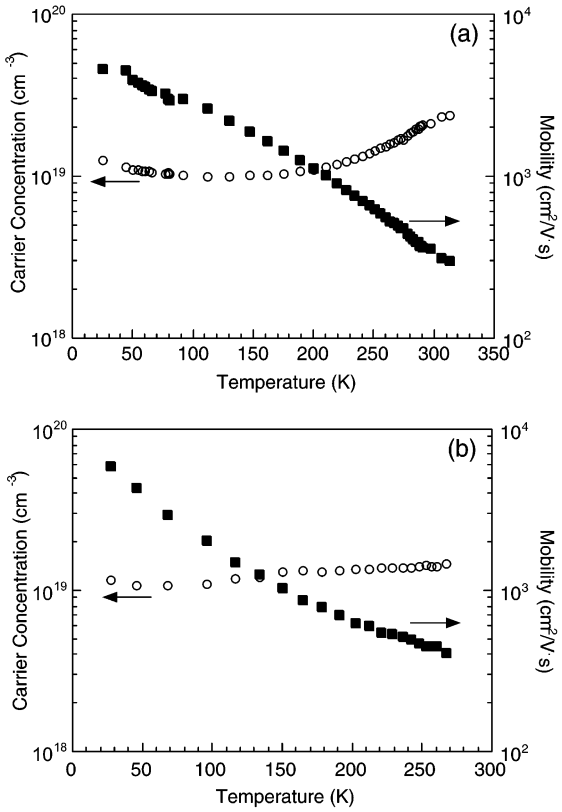

Figure 13. Carrier concentration and mobility as a function of temperature for (a) 0.5% Sn-doped and (b) 1.0% Te-doped $CsBi_4Te_6$ crystals.

of $CsBi_4Te_6$, reliable measurements of the thermal conductivity are needed. The rather complex and highly anisotropic crystal structure of $CsBi_4Te_6$ with the relatively large unit cell and heavy atoms is poised well to very high thermal resistance. This is because heavy atoms give rise to low acoustic phonon frequencies and the large unit cell and low symmetry generates relatively long and tortuous mean free paths in the structure. Therefore, a low thermal conductivity in this system can be expected.

The room-temperature thermal conductivities of oriented ingots of $CsBi_4Te_6$ measured along the *b*-axis are in the range of 1.25−1.85 W/m·K depending on the doping level, see Figure 14. These low values are comparable to ∼1.6 W/m·K of $Bi_{2-x}Sb_xTe_{3-y}Se_y$ alloy. The thermal conductivity expresses a significant anisotropic feature of $CsBi_4Te_6$, showing that the value measured along the perpendicular direction to the needle axis (*b*-axis) of the crystal is only about one-third of that obtained from the parallel (major conduction) direction.

The temperature dependence of the total thermal conductivity is typical for a crystalline material showing a large peak at ∼20 K which is due to the appearance of the Umklapp process as the temperature rises.[45] Over this temperature, heat-carrying phonons are involved in a number of collisions that begin to give rise to substantial thermal resistance that lowers the conductivity. At temperatures higher than ∼50 K, the lattice thermal conductivity (κ_{latt}) is not sensitive to the presence of very low levels of impurities such as dopants. Impurities are very important in the low-temperature region below the Umklapp peak in the thermal conductivity.

(45) Kittel, C. *Introduction to Solid State Physics*, 7th ed.; John Wiley & Sons: New York, 1996; ps 135, 162.

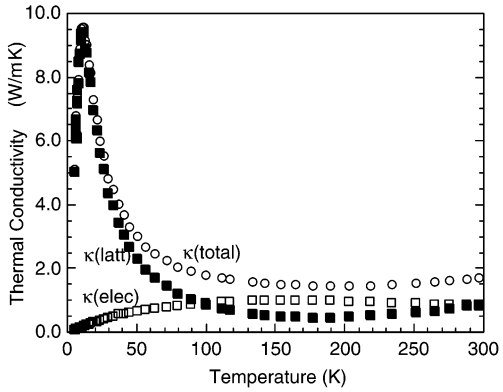

Figure 14. Variable-temperature thermal conductivities for oriented ingots of (a) "as-prepared" and 0.05% SbI_3-doped $CsBi_4Te_6$ measured (b) parallel and (c) perpendicular to the needle (*b*-axis) direction of the sample. For comparison, thermal conductivity data for the (d) $Bi_{2-x}Sb_xTe_{3-y}Se_y$ alloy are shown.

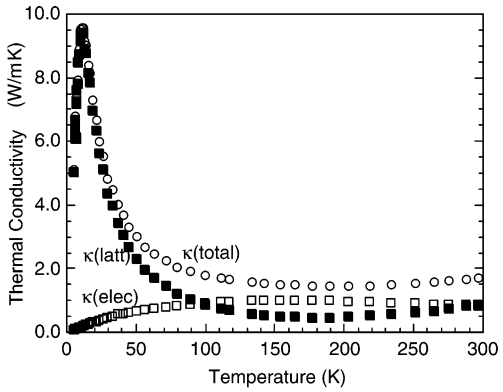

Figure 15. Variable-temperature total thermal conductivity (κ) for 0.05% SbI_3-doped $CsBi_4Te_6$, and both the lattice (κ_l) and the electronic (κ_e) contribution as estimated from the Wideman−Franz law.

The electronic thermal conductivity (κ_{elec}) can be estimated by using the electrical conductivity data in conjunction with the Wiedemann−Franz law[46] (Lorenz constant of 2.45×10^{-8} W·Ω/K^2 was used). The lattice thermal conductivity (κ_{latt}) can then be extracted by subtracting κ_{elec} from κ_{total}. The lattice thermal conductivity of $CsBi_4Te_6$ was estimated to 0.87 W/m·K at room temperature, see Figure 15, which is about 50% of the total thermal conductivity. This value was consistently obtained from a wide variety of doped $CsBi_4Te_6$ samples with varying numbers of carrier concentration and is reasonable because it is lower than the corresponding one for the Bi_2Te_3 which is 1.1 W/m·K.[47] The lower κ_{latt} in $CsBi_4Te_6$ is attributed to the lower symmetry crystal structure (*C*2/*m* vis-à-vis *R*-3*m*), the larger unit cell, and the ternary (vis-à-vis binary) composition of the compound. In the case of Bi_2Te_3, a considerable suppression of the κ_{latt} can be achieved via solid solutions (e.g., $Bi_{2-x}Sb_xTe_3$, $Bi_2Te_{3-y}Se_y$). Similarly, in $CsBi_{4-x}Sb_xTe_6$, $CsBi_4Te_{6-x}Se_x$, and $Cs_{1-x}Rb_xBi_4Te_6$, we expect a further decrease in κ_{latt} because the disordered atoms are expected to increase phonon scattering. Unfortunately, the range of *x* is more limited than in the Bi_2Te_3 system.

With a good assessment of the thermal conductivity at hand, the ZT of $CsBi_4Te_6$ samples was reasonably estimated. The ZT

(46) Kittel, C. *Introduction to Solid State Physics*, 7th ed.; John Wiley & Sons: New York, 1996; p 166.
(47) *CRC Handbook of Thermoelectrics*; Rowe, D. M., Ed.; CRC Press: Boca Raton, FL, 1995; pp 239, 429, 211 and references therein.

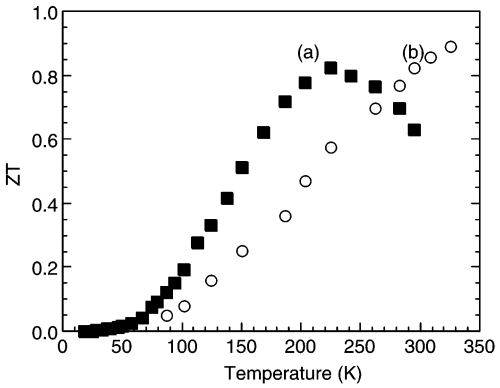

Figure 16. Comparison of ZT's for (a) 0.05% SbI_3-doped $CsBi_4Te_6$ and (b) p-type $Bi_{2-x}Sb_xTe_3$ alloy.

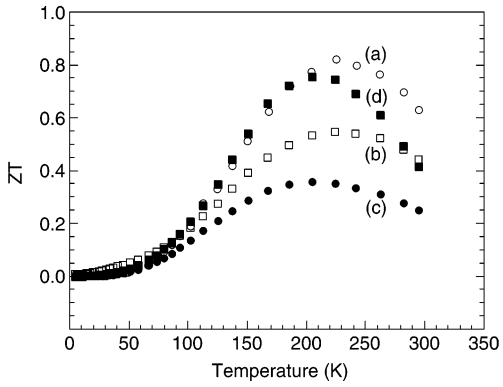

Figure 17. Variable-temperature ZT for (a) 0.05% SbI_3-doped $CsBi_4Te_6$ and for comparison the estimated ZT's for (b) 0.06% Sb-, (c) 0.3% BiI_3-, and (d) 0.1% Bi-doped sample.

values for the optimized p-type $CsBi_4Te_6$ and the commercial p-type $Bi_{2-x}Sb_xTe_3$ alloy are presented as a function of temperature in Figure 16. The highest ZT at present of 0.82 at 225 K for $CsBi_4Te_6$ was attained from 0.05% SbI_3-doped material. At room temperature, the ZT value is 0.65. The material with 0.06% Sb doped is also expected to have at least a comparable maximum ZT value to 0.82 of 0.05% SbI_3-doped material based on a higher power factor of 0.06% Sb-doped material. In contrast, commercially available $Bi_{2-x}Sb_xTe_3$ maximizes the ZT value at 0.95 near room temperature and drops to 0.58[48] at the temperature where the SbI_3-doped $CsBi_4Te_6$ shows its maximum ZT value of 0.82. Therefore, 0.05% SbI_3-doped $CsBi_4Te_6$ is expected to reach optimum performance at approximately ~75 K below that possible for the optimized $Bi_{2-x}Sb_xTe_3$. This suggests that $CsBi_4Te_6$ would be superior for thermoelectric applications to $Bi_{2-x}Sb_xTe_3$ in the low-temperature region.

The estimated ZT values were obtained for the high power factor samples of BiI_3-, Sb-, and Bi-doped $CsBi_4Te_6$, see Figure 17. Interestingly, 0.05% SbI_3- and 0.06 Sb-doped $CsBi_4Te_6$ have the same temperature, 225 K of maximum ZT, and 0.3% BiI_3- and 0.1% Bi-doped $CsBi_4Te_6$ also show the same corresponding temperature, 204 K. At this temperature region, the corresponding ZT of $Bi_{2-x}Sb_xTe_3$ is only about 0.42, and therefore $CsBi_4Te_6$ has the potential to outperform by ~100%. This is the lowest temperature we were able to achieve to date with our doping studies of this new material.

Electronic Band Structure of $CsBi_4Te_6$. Given the plethora of new charge-transport results presented above regarding both p-type and n-type doped samples of $CsBi_4Te_6$, the ability of this material to achieve high ZT values at low temperature justifies attempts to understand and rationalize the observed behavior in terms of its electronic band structure. Although a detailed band structure calculation has been published for $CsBi_4Te_6$,[18] here we will strive to make important links between the nature of the valence band maximum and the superiority of p-type samples and even speculate on the lack of comparable performance on behalf of the n-type samples and the corresponding nature of the conduction band.

Band structure calculations for $CsBi_4Te_6$ were performed without and with a spin−orbit coupling, see Figure 18. The spin−orbit coupling shifts the conduction band toward the valence band, resulting in an indirect gap of 0.04 eV placed between the Γ point in the valence band and a general point (C*) in the conduction band. Undoubtedly, $CsBi_4Te_6$ is a very narrow gap semiconductor. The band gap of $CsBi_4Te_6$ was observed spectroscopically in the far-infrared region to be ~0.1 eV, see Figure 19. This value agrees with the energy gap range of 0.04−0.08 eV obtained from the formula $E_g \approx 2S_{max} \cdot T_{max}$[49] using maximum thermopower and the temperature at maximum thermopower, based on the results of Figures 3 and 4. The band gap of Bi_2Te_3 is larger at 0.16 eV than that of $CsBi_4Te_6$. The

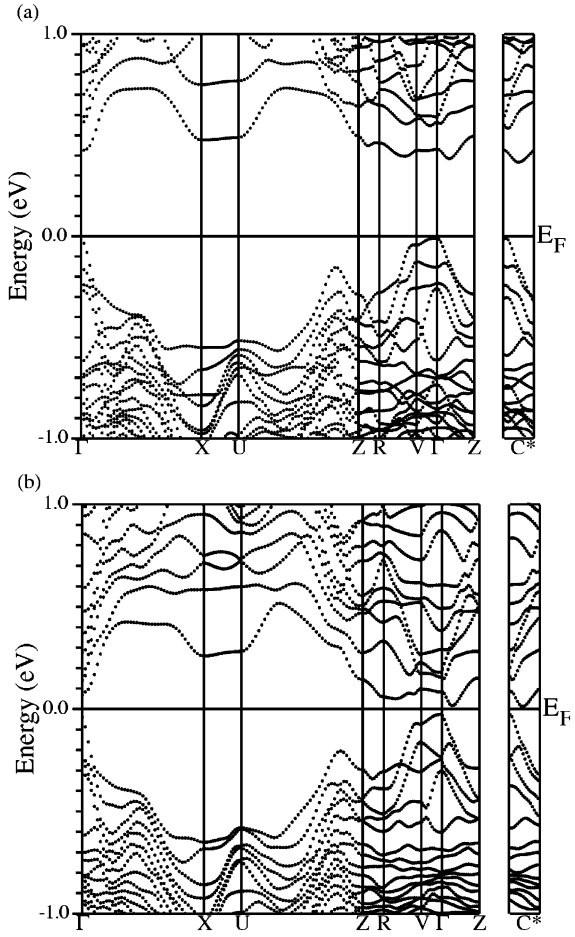

Figure 18. Electronic band structure of $CsBi_4Te_6$, (a) before adding spin−orbit interaction and (b) after adding spin−orbit interaction.

(48) Recent optimization work on p-type $Bi_{2-x}Sb_xTe_{3-y}Se_y$ alloys reported a low-temperature ZT_{max} value of 0.64 at ~210 K: Vedernikov, M. V.; Kutasov, V. A.; Luk'yanova, L. N.; Konstantinov, P. P. *Proceedings of the 16th International Conference on Thermoelectrics*; IEEE: Piscataway, NJ, 1997; p 56.

(49) Goldsmid, H. J.; Sharp, J. W. *J. Electron. Mater.* **1999**, *28*, 869.

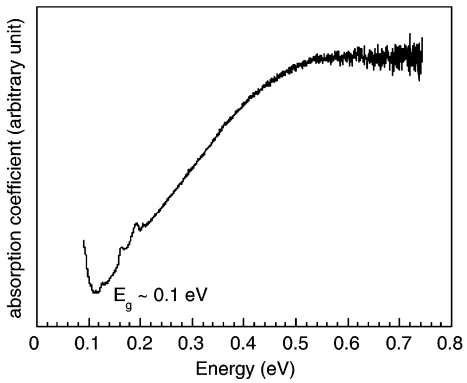

Figure 19. Infrared diffuse reflectance spectrum of $CsBi_4Te_6$. The energy gap is indicated in the spectrum.

energy gap of $CsBi_4Te_6$ calculated by electronic structure including spin−orbit interaction is also in good agreement with the value observed by angle resolved photoemission study.[50]

There are two key questions one would like to address in the case of $CsBi_4Te_6$. First, why is this material better at low temperatures than Bi_2Te_3? Second, what is the origin of high power factor and good thermoelectric performance? The answers may be found in examining the electronic band structure in detail. In general, it is well accepted that the temperature of the ZT maximum in thermoelectric materials is a function of band gap size: the wider the band gap, the higher the temperature of maximum achievable ZT. This is understood in terms of carrier excitation from the valence to the conduction band with temperature. Excitation across the gap generates carriers of sign opposite to those that are responsible for the high thermopower. The extra carriers have opposite thermopower, which tends to decrease the overall value through cancellation. Wider band gaps delay the onset of carrier excitation across the gap, and the ZT maximum can be attained at higher temperatures. This explains the observed temperatures for maximum ZT for Bi_2Te_3, PbTe, and SiGe which are 300, 500, and 1200 K, respectively, and the order that mirrors the band gap size of 0.15, 0.25, and 0.7 eV. The observed band gap of $CsBi_4Te_6$ of only ∼0.08−0.1 eV is the narrowest reported for a thermoelectric compound, and therefore it is not surprising that it performs best at low temperatures.

In general, when one moves from a binary semiconductor to a ternary one by introducing an alkali metal into its structure, the corresponding energy gap increases as the original structure is "broken down" and the overall dimensionality decreases. This is observed in almost every case with typical examples being CdS (2.4 eV) versus $K_2Cd_3S_4$ (3.0 eV),[51] SnS_2 (2.15 eV) versus $A_2Sn_4S_9$ (A = K, Rb, Cs) (2.66 eV),[52] and Bi_2Se_3 (0.32 eV) versus β-$K_2Bi_8Se_{13}$ (0.59 eV).[6] It is then surprising and puzzling that a ternary compound such as $CsBi_4Te_6$ would possesses a more narrow band gap than Bi_2Te_3. The answer to this lies in the presence of the Bi−Bi bond created by introduction of Cs metal into Bi_2Te_3. A detailed band examination near the Fermi level indicates that a significant contribution exists from p-orbitals associated with the Bi atoms participating in the Bi−Bi bond. In the absence of such a bond as in Bi_2Te_3, the empty p-orbitals of Bi are destabilized and can rise higher in energy, opening the gap. The Bi−Bi bonds are expected to be weaker than the Bi−Te bonds and the corresponding p-orbitals are not empty, so the destabilization is not great, resulting in a narrow gap, despite the presence of the alkali metals in the structure. The presence of such homoatomic bonds in semiconductors in fact seems to have a similar band narrowing effect. For example, in those cases that pairs of compounds exist where one has a homoatomic bond and the other does not, a similar trend is observed. In GaSe (Ga−Ga bond) and Ga_2Se_3 (no Ga−Ga bond), the former has a band gap of 1.1 eV whereas the latter has a gap of 2.0 eV. The same is observed in $BaGa_2Sb_2$ (Ga−Ga bond, E_g 0.34 eV) and GaSb (no Ga−Ga bond, E_g 0.69 eV).[53]

The second question regarding the origin of high thermoelectric performance in $CsBi_4Te_6$ may be addressed from a detailed examination of the shape of the bands near the Fermi level. Although this has been discussed extensively in an earlier publication, here we just give the essence of what follows from the calculations to tie in the experimental results. The band structure shows multiple band minima in the conduction band along ΓZ and RV directions and a single band maximum at the Γ point in the valence band. This indicates that $CsBi_4Te_6$ may have a large ZT when it is doped by an electron-donor reagent (n-type) because the number of band minima is proportionally related to the carrier effective mass and thus contributes to the thermopower.

The most noteworthy feature in the electronic structure of $CsBi_4Te_6$ is that the compound has a significant anisotropy in carrier effective masses. The anisotropic effective mass influences the B parameter[54] that is a material parameter proportionally related to ZT, and is defined as follows:

$$B = \frac{1}{3\pi^2}\left[\frac{2k_BT}{h^2}\right]^{3/2}\frac{\gamma\tau_x}{\kappa_l}\sqrt{\frac{m_y m_z}{m_x}} \qquad (1)$$

where m_x, m_y, and m_z are the effective masses along three principal directions, m_x is the effective mass along the direction of the current flow, γ is the band degeneracy, τ_x is the scattering time, and κ_l is the lattice thermal conductivity. It should be noted in eq 1 that m_x (the effective mass along the charge-transport direction) is inversely related to the parameter B. For an isotropic system where the effective masses along all three directions are similar, the B parameter will depend on only one of the effective masses (e.g., m_y) by cancellation of the other two (i.e., m_z/m_x). In contrast, for anisotropic system that the smallest effective masses are on the charge-transport direction x and one or both m_y and m_z are large, a large value of the B parameter can be expected. In the band structure of $CsBi_4Te_6$, along the direction (y) parallel to the Bi−Bi bonds, the carrier effective mass (m_y = 1.16) in the valence band is significantly higher than those in all other principal directions (m_x = 0.02, m_z = 0.09 for the valence band, m_x = 0.04, m_y = 0.47, m_z = 0.16 for the conduction band). This implies that effective hole transport

(50) An angle-resolved photoemission study on the electronic structure of $CsBi_4Te_6$ also showed 0.05 eV of energy gap: Greanya, V. A.; Tonjes, W. C.; Liu, R.; Olson, C. G.; Chung, D.-Y.; Kanatzidis, M. G. *Phys. Rev. B* **2002**, *65*, 205123.

(51) Papavassiliou, G. C.; Koutselas, I. B.; Mousdis, G. A.; Kapoutsis, J. A.; Axtell, E. A., III; Kanatzidis, M. G. in *Optical Properties of Semiconductor Nanostructures*; Sadawski, M. L., et al., Eds.; Kluwer Academic Publishers: The Netherlands, 2000; pp 97−100.

(52) Marking, G. A.; Evain, M.; Petricek, V.; Kanatzidis, M G. *J. Solid State Chem.* **1998**, *141*, 17−28.

(53) Kim, S.-J.; Kanatzidis, M. G. *Inorg. Chem.* **2001**, *40*, 3781−3785.

(54) (a) Hick, L. D.; Dresselhaus, M. S. *Phys. Rev. B* **1993**, *47*, 12727. (b) Hick, L. D.; Dresselhaus, M. S. *Phys. Rev. B* **1993**, *47*, 16631. (c) Hick, L. D.; Harman, T. C.; Dresselhaus, M. S. *Appl. Phys. Lett.* **1993**, *63*, 3230.

in the valence band takes place along the direction perpendicular to the crystal growth direction (crystallographic *b*-axis) in the plane of the Bi/Te slab, eventually leading to a tendency of $CsBi_4Te_6$ to be a p-type material. Also, Bi−Bi bonds play a significant role for a high ZT for $CsBi_4Te_6$.

Concluding Remarks

$CsBi_4Te_6$ is a promising new thermoelectric compound. The compound features a unique structure type with infinite [Bi_4Te_6] rods that are parallel-linked via Bi−Bi bonds. Bi−Bi bonds are rarely found in bismuth chalcogenide chemistry. It is one of very few compounds known that can be doped to achieve a very high ZT value below room temperature. The combination of several important characteristics such as low crystal symmetry (monoclinic), high structural anisotropy, large electronic anisotropy, heavy atoms, and large unit cell results in a system with very low thermal conductivity and an electronic structure that favors the development of high power factors. Band calculations suggested that $CsBi_4Te_6$ has very advantageous electronic structural features for a promising thermoelectric material characterized by a great deal of anisotropic effective mass. The electrical conductivity and thermopower are directly attributed to the elaborate electronic structure of a material near the Fermi level. The presence of Bi−Bi bonds in the structure is responsible for the material having a very narrow energy gap, nearly one-half that of Bi_2Te_3. In the absence of such bonds, the ternary system would have had a higher energy gap. The narrower band gap is related to the fact that the ZT maximum in $CsBi_4Te_6$ is achieved at lower temperatures than in Bi_2Te_3. $CsBi_4Te_6$ is very responsive to the type and level of doping agents. Low doping levels appear to more significantly affect the charge-transport properties of $CsBi_4Te_6$. The maximum ZT value of 0.82 at 225 K was achieved by doping with 0.05% SbI_3, which is among the highest values ever reported below room temperature. Also, from the 0.3% BiI_3-, 0.1% Bi-, and 0.06% Sb-doped materials, significantly high power factors were achieved around 150 K which is even 30−40 K below the temperature for the maximum power factor for the 0.05% SbI_3-doped material. This suggests that $CsBi_4Te_6$ may be useful for developing low-temperature thermoelectric devices and it could be adopted in a variety of applications with a wide range of working temperatures.

Acknowledgment. This work was supported at NU and MSU by the Office of Naval Research grant no. N00014-02-1-0867. Work at NU made use of the Central Facilities supported by the National Science Foundation through the NU Materials Research Center (DMR-9632472 and DMR-0076097).

Supporting Information Available: X-ray crystallographic files for $CsBi_4Te_6$ (CIF). This material is available free of charge via the Internet at http://pubs.acs.org.

JA039885F